INSTITUTO DE FÍSICA

preprint

IFUSP/P-271

ELECTRODISINTEGRATION EXPERIMENTS AND
VIRTUAL PHOTON THEORY

by

E. Wolynec

Instituto de Física, Universidade de São Paulo,
São Paulo, Brazil

UNIVERSIDADE DE SÃO PAULO
INSTITUTO DE FÍSICA
Caixa Postal - 20.516
Cidade Universitária
São Paulo - BRASIL

ELECTRODISINTEGRATION EXPERIMENTS AND VIRTUAL PHOTON THEORY

E. Wolynec

ABSTRACT

The virtual photon theory and experiments are reviewed. The point nucleus approximation and size effect corrections are discussed and compared with experimental results. The study of decay modes of giant resonances by electrodisintegration experiments is discussed and the experimental results are compared with the results from (e,e',x) and (α,α',x) coincidence experiments. New experimental results are presented.

Invited paper presented at the V Seminar on Electromagnetic Interactions of Nuclei at Low and Medium Energies , Moscow , USSR , June 15-17, 1981. (To appear in the Proceedings).

MAY/1981

ELECTRODISINTEGRATION EXPERIMENTS AND VIRTUAL PHOTON THEORY

E.Wolynec
Instituto de Física, Universidade de São Paulo, São Paulo, Brazil

Introduction

In inelastic electron scattering experiments nuclear excitations are studied by measuring the spectra of scattered electrons at some angle to the incident electron beam. This type of experiment integrates over all the final states of the nucleus; no information is obtained concerning the charged particles, neutrons or gamma rays emitted in the deexcitation of the nucleus. The complementary experiment, electrodisintegration, is to study these deexcitation products. This experiment integrates over all the final states of the electron.

Disintegration of nuclei by neutron emission has been extensively studied with quasi monochromatic gamma rays. However, the low intensity of anihilation beams requires the use of thick targets, preventing the study of nuclear deexcitation by emission of charged particles. The study of these deexcitation modes has been, so far, limited to electrodisintegration or to bremsstrahlung induced disintegration. In both cases the measurements integrate over a wide range of (virtual or real) photon energies. Electrodisintegration has been extensively used for this purpose. About 120 papers are available in the literature. Most of these measurements, which have been pioneered by the work of Barber and Vanhuyse /1/, refer to the (e,p) channel, but there are also several measurements of (e,α), (e,d), (e,t), (e,n), (e,f) and more recently pion electroproduction.

In an electrodisintegration experiment the cross section, $\sigma_{e,x}(E_o)$, for the emission of some particle x, is measured as a function of the incident electron energy, E_o, and then the energy dependence of the cross section is interpreted in terms of an appropriate photonuclear cross section. This technique has the advantage that it enhances quadrupole absorption by nuclei. While plane wave real photons have all multipoles in equal amounts, the virtual photons generated by the inelastically scattered electrons have an E2 component bigger than E1. By combining measurements of electro and photodisintegration it is possible to study the decay modes of E1 and E2 nuclear excitations.

Theory

A popular way of looking at electroexcitation is to consider the field produced at the nuclear site by the passing electron and analyse this into radiation multipoles, so that the effect on the

nucleus may be compared with that produced by electromagnetic radiation. In classical theory this is the well known method of Weizsäcker and Williams /2,3/ , while in quantum theory this is usually called the virtual photon method.

It may be helpful to review the approximations which are inherent in the virtual photon method. Of the radiation which originates from the electron, bremsstrahlung is that which escapes and can be detected at a distant point, for example by exciting a nuclear transition, and virtual radiation is that which is absorbed by the same nucleus from which the electron is scattering. Virtual radiation, in contrast to real radiation, is not a plane wave. Or, to put it in terms of the multipole decomposition, the spectrum does not contain the different multipole components in equal amounts, whereas the plane wave does. Labelling the multipoles by λ (which is E and M for electric or magnetic) and denoting by L the angular momentum, we may decompose the photoabsorption cross section in the form:

$$\sigma_\gamma(E) = \sum_{\lambda L} \sigma_\gamma^{\lambda L}(E) \tag{1}$$

Under suitable conditions, which will be examined in detail later, it is possible to reproduce the electroexcitation cross section, $\sigma_e(E_o)$, by calculating exactly as for bremsstrahlung photoexctiation, $\sigma_{br}(E_o)$, but substituting a virtual photon spectrum for the actual photon spectrum:

$$\sigma_e(E_o) = \int_o^{E_o-m} \sum_{\lambda L} \sigma_\gamma^{\lambda L}(E)\ N^{\lambda L}(E_o,E,Z)\ \frac{dE}{E} \tag{2}$$

while

$$\sigma_{br}(E_o) = \int_o^{E_o-m} \sum_{\lambda L} \sigma_\gamma^{\lambda L}(E)\ N(E_o,E,Z_r)\ \frac{dE}{E} \tag{3}$$

In the above equations $\sigma_\gamma(E)$ is the photoexcitation cross section as a function of photon energy. In eq.(2), $N^{\lambda L}(E_o,E,Z)$ is the virtual photon intensity spectrum produced by electrons of total energy E_o , inelastically scattered by a target nucleus of atomic number Z and in eq.(3), $N(E_o,E,Z_r)$ is the real photon intensity spectrum produced by electrons of total energy E_o, traversing a radiator of atomic number Z_r. Since the spectrum is independent of λL for real photons, eq.(3) reduces to:

$$\sigma_{br}(E_o) = N_r \int_o^{E_o-m} \sigma_\gamma(E)\ K(E_o,E,Z_r)\ \frac{dE}{E} \tag{4}$$

where we have used

$$N(E_o,E,Z_r) = N_r\ K(E_o,E,Z_r) \tag{5}$$

In eq.(5) N_r is the number of nuclei/cm^2 in the radiator and $K(E_o,E,Z_r)$ is the bremsstrahlung cross section.

Calculations of the virtual photon spectra in the plane wave Born approximation, assuming a point nucleus, were developed by Wick /4/, Thie et al. /5/ and Dalitz and Yennie /6/. Even though the plane wave approximation can only be used for very light nuclei, it will be used here to obtain the virtual photon spectra in order to discuss the approximations underlying the virtual photon hypothesis.

In plane wave Born approximation /7-12/ the cross section for the scattering of an electron of initial energy E_o and final energy E_f into a solid angle $d\Omega$ is:

$$\frac{d\sigma}{d\Omega} = \frac{4\pi e^2}{p_o^2} \sum_L \frac{(L+1)\, q^{2L}}{L\left[(2L+1)!!\right]^2} \left\{ \frac{L}{L+1} B(CL,q)\, V_C(\theta) + \left[B(EL,q) + B(ML,q)\right] V_T(\theta) \right\} \tag{6}$$

where the B's are the reduced transition probabilities and the dimensionless angular factors are:

$$V_C(\theta) = p_o p_f \frac{2p_o^2 + 2p_f^2 + 4m^2 - E^2 - q^2}{q^4} \tag{7}$$

$$V_T(\theta) = p_o p_f \frac{(p_o^2 + p_f^2 - E^2)\, q^2 - q(\vec{p}_o \cdot \vec{q})(\vec{p}_f \cdot \vec{q})}{q^2 (q^2 - E^2)^2} \tag{8}$$

and

$$E = E_o - E_f \tag{9}$$

$$\vec{q} = \vec{p}_o - \vec{p}_f \tag{10}$$

In the above equations: E is the excitation energy, p_o and p_f are the momenta associated with the energies E_o and E_f and q is the momentum transfer. The summation in eq.(6) extends from L=0 for the Coulomb multipoles (CL), and from L=1 for the transverse components.

The electron scattering cross section is dominated by small angle, low-q, transverse photon-like excitations owing to the $(q^2 - E^2)^2$ factor in the denominator of $V_T(\theta)$. This low-q dominance is not observed in electron scattering experiments which are usually performed at larger angles, where Coulomb and transverse terms are comparable. Since the electrodisintegration experiments integrate over all q's, the cross section is dominated by the very forward angles associated with low-q , $q \to E$.

The virtual photon spectrum /8,10/, essential to the interpretation of the electrodisintegration experiments, is obtained by comparing the electron scattering cross section of eq.(6) with the corresponding photonuclear cross section integrated over the level width:

$$\frac{dN^{\lambda L}}{d\Omega} = E \frac{d\sigma^{\lambda L}}{d\Omega} \Big/ \int \sigma_\gamma^{\lambda L}(E)\, dE \tag{11}$$

Since,

$$\int \sigma_{\gamma}^{\lambda L}(E)\, dE = 8\pi^3 \frac{(L+1)E^{2L-1}}{L[(2L+1)!!]^2} B(\lambda L,E) \tag{12}$$

and from eq.(6), the transverse components are:

$$\frac{d\sigma^{\lambda L}}{d\Omega} = \frac{4\pi e^2}{p_o^2} \frac{(L+1)q^{2L}}{L[(2L+1)!!]^2} B(\lambda L,q)\, V_T(\theta) \tag{13}$$

$$\frac{dN^{EL}}{d\Omega_T} = \frac{e^2}{2\pi^2} \frac{q^{2L}}{p_o^2 E^{2L-2}} \frac{B(EL,q)}{B(EL,E)} V_T(\theta) \tag{14}$$

$$\frac{dN^{ML}}{d\Omega} = \frac{e^2}{2\pi^2} \frac{q^{2L}}{p_o^2 E^{2L-2}} \frac{B(ML,q)}{B(ML,E)} V_T(\theta) \tag{15}$$

In the limit as $q \to E$, $B(\lambda L,q) \to B(\lambda L,E)$ so that the B's in the above expressions cancel.

In the long wave length approximation, $kR<<1$, it can be shown /8,12/ that:

$$B(CL,q) \xrightarrow[kR<<1]{} B(EL,q) \tag{16}$$

So the Coulomb part of the electron scattering cross section can also be related to the photonuclear cross section:

$$\frac{dN^{EL}}{d\Omega_L} = \frac{e^2}{2\pi^2} \frac{q^{2L}}{p_o^2 E^{2L-2}} \frac{L}{L+1} \frac{B(CL,q)}{B(EL,E)} V_C(\theta) \tag{17}$$

and in the limit $q \to E$ and $kR<<1$ the B's in the above expression also cancel. After cancellation of the B's in eq.(14), (15) and (17), the virtual photon spectra /5,6//13,14/ are obtained integrating over all angles of the scattered electron. The resulting virtual photon spectra in the point nucleus and plane wave Born approximation, for electric multipoles up to L=3 are:

$$N_T^{E1} = \frac{\alpha}{\pi}\left[\frac{E_o^2 + E_f^2}{p_o^2} \ell n \frac{E_o E_f + p_o p_f - m^2}{m(E_o - E_f)} - \frac{(E_o + E_f)^2}{2p_o^2} \ell n \frac{p_o + p_f}{p_o - p_f} - \frac{p_f}{p_o}\right] \tag{18}$$

$$N_L^{E1} = \frac{\alpha}{\pi}\left[\frac{(E_o + E_f)^2}{2p_o^2} \ell n \frac{p_o + p_f}{p_o - p_f} - \frac{p_f}{p_o}\right] \tag{19}$$

$$N_T^{E2} = \frac{\alpha}{\pi} \frac{E_o^2 + E_f^2}{p^2} \ell n \frac{E_o E_f + p_o p_f - m^2}{m(E_o - E_f)} \tag{20}$$

$$N_L^{E2} = \frac{8}{3}\left[\frac{p_f^2}{(E_o - E_f)^2}\right] \tag{21}$$

$$N_T^{E3} = \frac{\alpha}{\pi}\left[\frac{E_o^2 + E_f^2 - 4m^2}{p_o^2} \ell n \frac{E_o E_f + p_o p_f - m^2}{mE} + 2\frac{p_f}{p_o} \frac{E_o^2 + E_f^2 + E_o E_f - 3m^2}{(E_o - E_f)^2}\right] \tag{22}$$

$$N_L^{E3} = \frac{\alpha}{\pi}\frac{p_f}{p_o}\,\frac{E_o E_f(3E_o^2 - 2E_oE_f + 3E_f^2) + m^2(5E_o^2 - 6E_oE_f + 5E_f^2) - 8m^4}{(E_o - E_f)^4} \qquad (23)$$

The subscripts T and L refer to the components perpendicular and parallel to the direction of momentum transfer q, and

$$N^{EL} = N_T^{EL} + N_L^{EL} \qquad (24)$$

The plane wave virtual photon spectra provide a useful guide, but experimental results /13-17/ showed that it could only be used for very light nuclei. Onley and his collaborators /18,19/ have calculated the virtual photon spectra in the distorted wave Born approximation, DWBA, that is, taking into account the distortion of the incoming and outgoing electrons in the Coulomb field of a point nucleus. As in the simple Born approximation expressions for the virtual photon distributions, the assumption of a point nucleus is a necessary step in order to make the nuclear matrix elements which govern photo and electroexcitation identical.

The effect of taking into account Coulomb distortion is illustrated in Fig. 1, which compares E1 and E2 virtual photon spectra calculated in plane wave (PW) and distorted wave approximation (DWBA), produced by 10 MeV electrons scattered by a Uranium nucleus /20/. The E2 virtual photon spectrum, already enhanced with respect to the E1 in the plane wave solution, is further enhanced when distortion is taken into account. Fig. 2 shows DWBA E1 virtual photon spectra for 27.5 MeV electrons and positrons scattered by targets of various atomic numbers. To obtain the spectra for positrons it is merely necessary to reverse the sign of the interaction and hence it is equivalent to making Z negative. The distortion effects, which increase with Z, are much larger for electrons than for positrons. Because positrons are repelled by the nucleus whereas electrons are attracted, the amplitude of a positron wave function is generally smaller in the neighborhood of the nucleus than that of an electron of comparable energy. The DWBA calculation for $Z = \pm 1$ reproduces the plane wave result.

In obtaining the virtual photon spectra it was necessary to take the limit $q \to E$ in order to cancel the nuclear matrix elements ocurring in N_T^{EL} and N^{ML}. Because the main contribution to the integrals over the electron scattering angles comes from rather small angles, this approximation can be valid for the majority of the transitions, even though the primary electron energy is high. However, in order to make $B(CL,q) \to B(EL,E)$ we had to take a more restrictive limit: $kR \ll 1$. Since this was a necessary step in order to obtain N_L^{EL}, it

is reasonable to expect that the point nucleus approximation will fail when N_L^{EL} becomes dominant. Fig. 3 shows the ratio of the number of 16.6 MeV longitudinal to transverse virtual photons in the PWBA E1 and E2 spectra as a function of electron energy. The longitudinal parts never make an important contribution to the E1 virtual photon spectra, but the longitudinal components of the E2 become as large as the transverse for electrons of energy near 50 MeV. Corrections to the virtual photon spectra due to the finite size of the nucleus have been considered by Barber /13/, Barber and Wiedling /14/ and Isabelle and Bishop /21/. If the long wave lenght limit is not satisfied, then the values of $N^{\lambda L}$ will depend upon the physical details of the nucleus and so $N^{\lambda L}$ will become model dependent. This of course reduces the attractiveness of using the virtual photon concept for data analysis, but if a simple model could be used to take account of finite nuclear size, then the concept could be extended to higher electron energies. Corrections based on a simple model have been proposed by Dodge and his collaborators /22,23/ and by Shotter /24/.

The correction suggested by Dodge et al. is based on the fact that the transition probabilities, $B(\lambda L,q)$, ocurring in the electron scattering cross section vary with q as the squares of the spherical Bessel functions, $j_L(qR)$, as far as q is not close to a diffraction minimum. It consists in multiplying $N^{\lambda L}(E_o,E,Z)$ by a quantity

$$F^{\lambda L}(qR) = \left[\left(\frac{E}{q}\right)^L \frac{j_L(qR)}{j_L(ER)} \right]^2 \qquad (25)$$

with $R = (3/5)^{1/2} R_o = 0.93 A^{1/3}$ F. The average values of q participating in the interaction are estimated using the plane wave virtual photon spectra:

$$\frac{\langle q \rangle^2}{E^2} \cong \frac{\langle q^2 \rangle}{E^2} = \frac{N_T^{E(L+1)} + \left[L(L+2)/(L+1)^2\right] N_L^{E(L+1)}}{N^{EL}} \qquad (26)$$

In order to obtain $\langle q^2 \rangle$ from eq.(26) one has to assume that the B's in eq.(14), (15) and (17) cancel, which means one has to assume $qR \ll 1$. Consequently this correction is only valid for small q.

Shotter /24/ has suggested a correction based on the generalized Helm model /25,26/ also using the plane wave approximation. The results of this correction are illustrated in Figs. 4 and 5. In these figures the number of 10 MeV longitudinal (curves L) and transverse (curves T), E1 and E2 virtual photons are shown as a function of electron energy for various A. The values for A=1 correspond to a point nucleus. The correction suggested is to multiply $N^{\lambda L}(E_o,E,Z)$ by:

$$F^{\lambda L}(E_o,E,A) = N^{EL}(E_o,E,A)/N^{EL}(E_o,E) \qquad (27)$$

where $N^{EL}(E_o,E)$ is the plane wave spectrum for a point nucleus. The isochromates shown in Figs. 4 and 5, that is $N_T^{EL}(E_o,10,A)$ and $N_L^{EL}(E_o,10,A)$, were obtained substituting in eq. (14), (15) and (17)

$$\frac{B(EL,q)}{B(EL,E)} = \left[\left(\frac{q}{E}\right)^{L+1} \frac{j_L(qR)}{j_L(ER)} \right] \qquad (28)$$

and

$$\frac{B(CL,q)}{B(EL,E)} = \left[\left(\frac{q}{E}\right)^{L} \frac{j_L(qR)}{j_L(ER)} \right] \qquad (29)$$

and using $R = 1.2\ A^{1/3}\ F$.

Both correction factors $F^{\lambda L}$ given by expressions (25) and (27) yield the same result as far as $\langle q \rangle$ in eq.(26) is small.

It is not surprizing that both corrections yield about the same answer because in both cases the ratio of the transition probabilities ocurring in electro and photoexcitation is represented in the same way. The main difference between them is that in eq.(25) an average value of $\langle q \rangle$ is used and in (27) the correction is applied to $\frac{dN}{d\Omega}$ and it is integrated over all possible values of q. In principle the correction suggested by Shotter should be valid for a broader range of q . Fig. 6 shows $F^{\lambda L}$ obtained from eq.(25) and (27) for 10 MeV E1 and E2 virtual photons as a function of the electron energy, for A=240 and A=50.

Experimental tests of the virtual photon method

There has been several /13-17/ /27-29/ experimental tests of the E1 virtual photon spectra. The predictions of the DWBA calculations have been verified /20/30/31/ in experiments in which the ratio of cross sections produced by electrons and positrons and the ratio of cross sections produced by electrons and bremsstrahlung photons were obtained. It has also been shown /32/ that the cross section for the reaction $^{238}U(e,n)^{237}U$ bears the proper relationship to the $^{238}U(\gamma,n)^{237}U$ cross section. As examples of the agreements between experimental data and the DWBA calculation of E1 virtual photon spectra we show Figs. 7 to 9.

Fig. 7 shows the ratio of cross sections produced by 27.5 MeV electrons and positrons, σ^-/σ^+ , as a function of the target atomic number Z . Fig. 8 shows the same ratio for the fission cross section in ^{232}Th as a function of electron and positron incident energy /33/. The solid curve in each figure is the result of the DWBA calculation. Apart from the fact that positrons are repelled by the nucleus whereas

electrons are attracted, in all other respects the eletromagnetic interactions of positrons and electrons are identical. Hence the difference in electron and positron cross sections has little to do with nuclear physics and is a consequence solely of electrodynamics. The agreement between the experimental data and the DWBA calculation is a test of the accuracy of the distorted wave calculation and also of the approximations underlying the virtual photon hypothesis.

Fig. 9 shows the ratio of measured to calculated $\sigma_{e,n}(E_o)$ in ^{238}U as a function of electron incident energy E_o. $\sigma_{e,n}(E_o)$ was calculated using in eq.(2) the DWBA El virtual photon spectrum and the $\sigma_{\gamma,n}$ cross section measured by Veyssière et al. /34/ and by Dickey and Axel /35/. The agreement between the measured cross section, $\sigma_{e,n}$, and the calculated value, $\sigma^{El}_{e,n}$, shown in Fig. 9 lacks only a 4% normalization of the cross section magnitudes which is well within the errors of the $\sigma_{e,n}$ and $\sigma_{\gamma,n}$ absolute measurements. From this result we can conclude that the virtual photon calculation in the point nucleus approximation is good for El excitations in uranium up to electron energies of at least 25 MeV and even higher energies for lighter nuclei.

All the above experimental tests used the excitation of the El Giant Resonance, so they were integrated over a broad range of photon energies. The maximum energy used was $\sim$ 40 MeV so these tests were insensitive to nuclear size effects. If we apply the size effect corrections discussed in the previous section to the calculated curve of Fig. 7, it would lower the curve by 2% for Z=90.

In order to test the El virtual photon calculation in more detail as well as size effects, Dodge, Wolynec and Hayward are measuring the electroexcitation of the 16.3 MeV analogue state in ^{90}Zr as a function of electron incident energy.

The 16.3 MeV state in ^{90}Zr is a well known El state which decays emitting protons to the ground state /36/37/ and to the 1.51 MeV excited state of ^{89}Y /38/. Fig. 10 shows the differential cross section, $d^2\sigma/d\Omega dT$, for the electroproduction of protons from ^{90}Zr at 90° by incident electrons of 60 MeV versus the proton kinetic energy T_p. Peak A is the decay of the 16.3 MeV state to the ground state of ^{89}Y. In Fig. 11 the 90° differential cross section, $d^2\sigma/d\Omega dT$, is shown for 19.4 MeV electrons, and for proton kinetic energies around the analogue state. The curve through the points shows the fit of a Gaussian plus a quadratic function for the continuum, used to obtain the cross section $\frac{d\sigma}{d\Omega}$ for the analogue state.

The radiation width Γ is related to the integrated photo-absorption cross section:

$$\int_{\text{level width}} \sigma_\gamma \, dE = (\pi\lambda\!\!\!^{-})^2 \, \frac{2I_K + 1}{2I_o + 1} \, \Gamma \qquad (30)$$

where I_o and I_K are the spins of initial and final states.

Since the virtual photon theory relates photo and electroexcitation through:

$$\int_{\text{level width}} \sigma_\gamma \, dE = \frac{\sigma_e(E_o)}{N^{\lambda L}(E_o,E,Z)/E} \qquad (31)$$

then,

$$\Gamma = \frac{(2I_o+1)\sigma_e(E_o)}{(\pi\lambda\!\!\!^{-})^2(2I_K+1)N^{\lambda L}(E_o,E,Z)/E} \qquad (32)$$

The radiation width can be obtained from the measured values of $\sigma_{e,p}(E_o)$, using eq.(32). If the shapes of the virtual photon spectra are correct, the values of the radiation width obtained will be independent of E_o. Figs. 12-a) and b) show the values obtained for Γ as a function of E_o derived using the DWBA E1 virtual photon spectra without and with size effect correction, respectively.

Since there are no size effects for real photons, a radiator was interposed in the beam ahead of the target, in order to measure the excitation of the 16.3 MeV state by bremsstrahlung photons for electron energies in the range 50-106 MeV. The value of Γ derived from these measurements is $\overline{\Gamma} = 57.3 \pm 0.8$ eV which is in good agreement with the value of 54 ± 13 eV from the proton capture work of Hasinoff et al. /36/. The dashed lines in Fig. 12 a) and b) show the average value of Γ derived from our bremsstrahlung data. The values of Γ derived from the electroexcitation measurements are in good agreement with the value obtained from the bremsstrahlung data if the size effect correction is applied to the virtual photon calculation. Here, both Shotter's and Dodge's correction give nearly the same results. The results shown in Fig. 12 b) where obtained using Shotter's correction (eq.(27)), which gives $\overline{\Gamma} = 56.7 \pm 0.9$ eV, while Dodge's correction gives $\overline{\Gamma} = 56.2 \pm 0.9$ eV.

These preliminary results show that the virtual photon calculation of the E1 spectrum is in good agreement with experiment within a few percent. The size effect corrections discussed in the previous section are of the right magnitude. The experiment should be pushed to higher energies where the size effect correction becomes more important.

Electrodisintegration experiments

It is not our purpose to review here all the electroproduction work available in the literature, but to give an overall idea of the

type of work that has been carried out. We will concentrate in the more recent experiments in which measurements of electrodisintegration are used to study the decay modes of the Giant E2 Resonance.

The first electrodisintegration experiment was performed by Collins /39/40/ observing neutrons emitted from ^{9}Be. This experiment has been extended by Barber /13/. The same author and his collaborators subsequently studied the angular distributions of protons ejected by electrons of energy up to $\sim$ 40 MeV from Nb, In, Ta and Au /1/, ^{12}C /41/, ^{12}C, ^{16}O, ^{19}F, Ne and ^{27}Al /42/, covering the Giant Resonance region of these nuclei. The ejection of protons, deuterons, tritons, ^{3}He and ^{4}He by electrons of energy up to 90 MeV was studied by Hutcheon /43/. Proton spectra and angular distributions from ^{12}C using 200 MeV electrons were measured by Vysotskaya /44/ and protons from the decay of ^{12}C and ^{13}C Giant Resonance using 46 MeV electrons were observed by Wong /45/.

The proton yields from electron bombardment of ^{207}Pb, ^{209}Bi, ^{139}La, ^{141}Pr and ^{148}Sm have been used by Shoda /46/47/ to determine the radiative widths of isobaric analog states in these nuclei. The same author and his collaborators have measured high resolution proton energy spectra and studied in detail their excitation functions for several medium weight and heavy nuclei, in an extensive study of isobaric analog resonances and of the isospin splitting of the Giant El Resonance.

In most of the papers on electroproduction the measured electrodisintegration cross section was assumed to be a pure El process. The electrodisintegration cross section was then unfolded with the El plane wave spectrum in eq.(2) in order to obtain the corresponding photodisintegration cross section, which is used to interpret the physics involved in the process under study. It is evident from Figs. 1 and 2 that for heavy nuclei the use of the plane wave El spectrum will lead to a wrong magnitude and shape of the photo cross section.

The worst source of uncertainty in the photodisintegration cross section derived from electrodisintegration measurements is not the use of the plane wave calculations, but the assumption of a pure El process, which was used in most of the published work found in literature. To illustrate this point, Fig. 13 shows the El and E2 virtual photon spectra for 25 MeV electrons scattered from a Uranium nucleus. The E2 spectrum is about one order of magnitude bigger than the El for virtual photon energies in the region of the isoscalar E2 resonance. Even though the isoscalar E2 integrated strength is only a few percent of the El integrated strength, the large enhancement of the E2 component by electrons in heavy nuclei make them contribute

with about the same intensity.

We will discuss an example of how the pure E1 assumption could lead to the wrong interpretation of the physical phenomena under study. The data selected was chosen due to the high resolution and fine energy steps of the measurements. Many similar examples can be found in reviewing the available electroproduction data.

Suzuki and Shoda /48/ obtained the photoproton cross section, $\sigma_{\gamma,p}$, for ^{181}Ta by unfolding their measured (e,p) cross section with the plane wave E1 virtual photon spectrum. Fig. 14 shows their proton energy spectra at 90° and several electron incident energies. In Fig. 15 the resulting yield curve is shown versus the electron incident energy E_o. The interesting feature is that above 20 MeV a new proton group appears in the energy spectra producing a second peak at $E_p \cong 12$ MeV. A break is observed in the proton yield around 20 MeV. The unfolding of this yield results in a resonance peaking at ∿21 MeV, shown in Fig. 16, which presents the photoproton cross section, $\sigma_{\gamma,p}$, versus the photon energy E. This resonance was interpreted as the T upper component of the E1 Giant Resonance. However the angular distribution of the protons, studied in the early work of Barber and Vanhuyse /1/ do not support a pure E1 assumption. Fig. 17 shows the angular distribution of protons having energies in the region of the second maximum. The angular distribution is strongly forward peaked, suggesting an interference of two multipoles of opposite parity, probably E1-E2. Furthermore the resonance found at 21 MeV is in the region where the Isovector E2 Resonance is expected to be in ^{181}Ta. It is conceivable that the structure at 21 MeV, instead of being the T upper component of the E1 resonance, could be the decay of the isovector E2 by proton emission. The ambiguity between both interpretations, pure E1 versus E1+E2 can be resolved by measuring the bremsstrahlung yield as well as the electrodisintegration, as in the experiments described in the next section.

Study of E2 components using electroexcitation

As discussed earlier the virtual photon concept can be used as far as $qR<<1$ is satisfied. For bombarding energies such that the theory can be used in the analysis of data the electrodisintegration is insensitive to monopole excitations. High momentum transfer is required to excite monopole states and since electrodisintegration experiments integrate over all scattering angles they are dominated by low q.

Hayward /23/ has discussed the excitation of monopole and also E3 in electrodisintegration experiments and showed that the excitation of both modes for electron energies up to 50 MeV can be neglected.

Fig. 18 shows the distorted wave E1, E2 and E3 virtual photon spectra generated by 50 MeV electrons scattered from a Ni nucleus. The E3 spectrum is even more enhanced than the E2 relatively to the E1 . However the integrated strength of an E3 sum is about 0.1% of that of an E1 sum and the enhancement of the E3 spectrum is not enough to make experiments in the energy region considered here sensitive to E3 excitations.

Fig. 19 illustrates the enhancement of E2 components in electroexcitation. The curves shown are functions that fit measured angular distributions of fission fragments produced by 6 MeV electrons /49/50/, curve (e,f), and by bremsstrahlung of end point energy 6 MeV /51/, curve (γ,f). The functions fitted in both cases are: $f(\theta) = a + b \sin^2\theta + c \sin^2 2\theta$. The E2 strength derived from both experiments is the same, but while the (γ,f) is dominated by the E1 excitation, the (e,f) is clearly dominated by E2.

There are some very interesting experiments that illustrate the exploitation of the virtual photon technique in the study of fission. For example, using electrons in the energy range 20-120 MeV, Shotter et al. /52/ have shown that the ^{238}U(e,f) cross section rises too steeply to be an electric dipole phenomenon only. They showed that there must be an important E2 absorption resulting in fission, but from their experiment it was not possible to tell whether it was located at the energy of isoscalar or isovector resonance.

In a series of detailed experiments Arruda Neto and his collaborators /49/50/53-57/ studied the electrofission of ^{238}U, ^{236}U and ^{234}U. We will describe in some detail the analysis of ^{238}U(e,f) data to illustrate how the E2 component in the photonuclear cross section can be obtained.

Assuming that the only important multipoles in the electrofission cross section are E1 and E2, the photofission cross section is:

$$\sigma_{\gamma,f}(E) = \sigma^{E1}_{\gamma,f} + \sigma^{E2}_{\gamma,f} \qquad (33)$$

Then the measured electrofission cross section, $\sigma_{e,f}(E_o)$, can be related to the measured photofission cross section, $\sigma_{\gamma,f}(E)$, by:

$$\sigma_{e,f}(E_o) = \int_o^{E_o-m} \left[\sigma^{E1}_{\gamma,f}\, N^{E1}(E_o,E,Z) + \sigma^{E2}_{\gamma,f}(E)\, N^{E2}(E_o,E,Z)\right] \frac{dE}{E} \qquad (34)$$

Since $\sigma_{\gamma,f}(E)$ has been measured with quasi monochromatic γ-rays /34/35/, expression (34) with the use of (33) can be rewritten as:

$$\sigma_{e,f}(E_o) = \int_o^{E_o-m} \sigma_{\gamma,f}(E)\, N^{E1}(E_o,E,Z)\, \frac{dE}{E} +$$

$$+ \int_o^{E_o-m} \sigma^{E2}_{\gamma,f}(E) \left[N^{E2}(E_o,E,Z) - N^{E1}(E_o,E,Z)\right] \frac{dE}{E} \qquad (35)$$

The first integral in the above expression can be calculated using

the experimental values of $\sigma_{\gamma,f}(E)$ available in the literature /34/35/36/. One can obtain

$$Y(E_o) = \sigma_{e,f}(E_o) - \int_o^{E_o-m} \sigma_{\gamma,f}(E)\ N^{El}(E_o,E,Z)\ \frac{dE}{E} \qquad (36)$$

From (35) and (36)

$$Y(E_o) = \int_o^{E_o-m} \sigma^{E2}_{\gamma,f} \left[N^{E2}(E_o,E,Z) - N^{El}(E_o,E,Z)\right] \frac{dE}{E} \qquad (37)$$

and $\sigma^{E2}_{\gamma,f}(E)$ can be obtained by unfolding the quantity $Y(E_o)$. To obtain $Y(E_o)$ from expression (37), in this particular case, two experimental cross sections were used, $\sigma_{\gamma,f}(E)$ and $\sigma_{e,f}(E_o)$, which were measured at different laboratories and may differ in absolute value. To take this into account a few points of the photofission cross section produced by bremsstrahlung photons, $\sigma_{br,f}$, were measured. Comparing the measured $\sigma_{br,f}$ with the calculated values:

$$\sigma_{br,f}(E_o) = N_r \int_o^{E_o-m} \sigma_{\gamma,f}(E)\ K(E_o,E,Z)\ \frac{dE}{E} \qquad (38)$$

the difference in absolute values can be assessed. In the ^{238}U experiment, the ratio between measured to calculated $\sigma_{br,f}(E_o)$ was 1.04 .

Fig. 20 shows the measured (e,f) cross section for ^{238}U as a function of electron energy. The full curve is the calculated $\sigma_{e,f}$ cross section for a pure El process. The difference between the experimental points and the calculated curve gives $Y_{e,f}(E_o)$ shown in Fig. 21. The E2 component of the photofission cross section, $\sigma^{E2}_{\gamma,f}(E)$, was obtained unfolding $Y_{e,f}(E_o)$ and is shown in Fig. 22.

Table 1 summarizes the results obtained in São Paulo for the 3 uranium targets. The decay of the E2 isoscalar resonance by fission has also been studied in (α,α',f) coincidence experiments /58,59/ and in a $(^6Li,^6Li',f)$ experiment /60/. Their results are summarized on Table 2. In Table 1 the photofission cross section, $\sigma_{\gamma,f}$, derived from the electrofission experiment, was converted into strength function in order to allow comparison with the hadron scattering result. In both tables the values of the fission probability, Γ_f/Γ, were evaluated at the peak energy and in Table 2 the peak energy was deduced from the singles spectra.

Table 1

E2 component in the fission channel derived from (e,f) experiments

Nucleus	Strength Function		Percentage of EWSR	$\frac{\Gamma_f}{\Gamma}$ (%)	Ref.
	Peak Energy (MeV)	FWHM (MeV)			
^{234}U	8.2 ± 0.4	4.8 ± 1.0	87 ± 14	70 ± 15	55
^{236}U	8.9 ± 0.4	4.7 ± 1.0	72 ± 10	60 ± 10	54
^{238}U	8.3 ± 0.4	5.0 ± 1.0	55 ± 10	40 ± 10	53

Table 2

E2 component in the fission channel derived from the hadron scattering coincidence experiments for ^{238}U

Nucleus	Strength Function		Percentage of EWSR	$\frac{\Gamma_f}{\Gamma}$ (%)	Ref.
	Peak Energy (MeV)	FWHM (MeV)			
(α,α',f)	∿11	4 ± 0.5	-	<10	58
(α,α',f)	10.6	2.2 ± 0.2	50 ± 15	25 ± 10	59
(^{6}Li,^{6}Li',f)	∿10.5	∿7	-	≳20	60

The discrepancy between the various hadron scattering results can be understood by the difficulty of the experiment, a major source of uncertainty arising from the subtraction of the substantial nuclear backgrounds. This is illustrated in Fig. 23 where the coincidence spectra from the work of Bertrand et al. /59/ is shown. In Fig. 23 the top part shows the inelastic alpha spectra from the reaction $^{238}U(\alpha,\alpha',f)$ for the indicated angles. Contaminants are shown cross hatched. At 11.5 degrees, the deduced shape of the giant resonance peak and the underlying continuum are shown as solid curves. In the middle part of Fig. 23 the spectra of alpha particles measured in coincidence with fission fragments is shown. In the 11.5 degrees spectrum an enhancement indicated by the smooth curve is attributed to fission decay of the K=0 component of the GQR. In the bottom part of Fig. 23 the fission probability for the (α,α',f) reaction is shown. B_f is the fission threshold; S_n is the neutron separation energy for ^{238}U; nf and 2nf indicate the energies for the onset of

second and third chance fission. Even though the result obtained by Bertrand et al. exhausts the same amount of E2 strength as the São Paulo result, there is a serious disagreement between the hadron induced fission experiments and the electrofission results:the strength function obtained from hadron induced experiments is zero bellow 8 MeV and peaks at a higher energy.

In order to understand the different results obtained in the various experiments for the fission decay of the isoscalar E2 resonance, the (e,e',f) cross section is being studied at Stanford /61/. Figs. 24 and 25 show their coincidence spectra for electrons of 80.1 and 117.7 MeV, scattered at 40 degrees as a function of the excitation energy, E , of the nucleus. The fission fragments are integrated over all angles. The solid curve is the E1 contribution which is calculated using the known photofission cross section, $\sigma_{\gamma,f}(E)$. The calculated E1 is an upper limit, which will yield a lower limit for the E2 component. The E2 strength function obtained from these preliminary results is shown in Fig. 26. The solid curve, with its uncertainty indicated by the dashed curves, is the strength function derived from the São Paulo experiment. There is good agreement between both results, with a difference in magnitude that could be caused by discrepancy in the absolute values. The agreement between the São Paulo electrofission result and the Stanford (e,e',f) can be viewed as the first available experimental test of the E2 virtual photon spectrum.

In cases where the photonuclear cross section has not been measured, the E1 and E2 components can be obtained combining measurements of electrodisintegration with photodisintegration induced by bremsstrahlung photons. Exploiting this idea we have studied /22/ the E1 and E2 component in (e,α) and (e,p) reactions for several medium weight nuclei.

In these experiments we measured the spectra of protons and α particles at several angles, produced by electrons in the range 16-100 MeV. Figs. 27 and 28 show proton and alpha particle spectra at 90° from ^{64}Zn bombarded by 30 MeV electrons. These spectra were then integrated over outgoing particle energy and angle to obtain the cross sections $\sigma_{e,x}(E_o)$.

In this type of experiment,additional very useful information can be obtained if a radiator is interposed in the electron beam ahead of the target so that the outgoing particles are now generated by electrodisintegration plus the bremsstrahlung from the radiator. The advantage of this method is that it allows us to change the relative contribution of the various multipoles participating in the reaction.

For electrons of energy higher than 35 MeV a second experiment was performed. A radiator, 217 mg/cm^2 of Ta, was interposed in the beam

7.6 cm ahead of the target but out of view of the spectrometer.

Fig. 29 and 30 show the measured (e,α) and (e,p) cross sections as a function of total incident electron energy E_o (open circles). The full circles represent the yield, $Y_{e,x}(E_o)$ obtained when a 0.217 g/cm^2 Ta radiator was placed in the electron beam ahead of the target.

The relationship between our measured electrodisintegration cross section and the corresponding photodisintegration cross section is given by eq.(2). The corresponding expression for the yield with the radiator is:

$$Y_{e,x}(E_o) = \sigma_{e,x}(E_o - 2\Delta E_o) + N_r \int_o^{E_o - m} \sum_{\lambda L} \sigma_{\gamma,x}^{\lambda L}(E)\, K(E_o - \Delta E_o, E, Z)\, \frac{dE}{E} \qquad (39)$$

where ΔE_o is the energy an electron loses in traversing half the radiator thickness and for K we have used the Davies-Bethe-Maximon /62/ bremsstrahlung cross section.

The cross sections, $\sigma_{e,x}(E_o)$ and the yields of photo plus electrodisintegration, $Y_{e,x}(E_o)$, have been simultaneously fitted using E1 and E2 virtual photon spectra. Because in our experiment we do not have enough points at small energy intervals, instead of unfolding the cross sections as in the São Paulo experiment, we represent $\sigma_{\gamma,x}^{\lambda L}$ by histograms. The resulting histrograms for $\sigma_{\gamma,x}^{E1}$ and $\sigma_{\gamma,x}^{E2}$ are shown in Figs. 29 and 30 (right hand scale).. The smooth curves through the data points result from combining the histograms, representing the E1 and E2 (γ,x) cross sections in eq.(2) and (39) with the E1 and E2 virtual photon spectra.

It is impossible to fit the electrodisintegration cross section $\sigma_{e,x}(E_o)$ and the yield $Y_{e,x}(E_o)$ with pure E1 multipolarity. However it is always possible to fit the electrodisintegration only with pure E1. To illustrate the importance of measuring the photodisintegration yield for at least a few points, in Fig. 31 we show the result of fitting only the electrodisintegration and assuming pure E1. The curve above the full circles is the predicted $Y_{e,\alpha}(E_o)$. It is clear from Fig. 31 that the pure E1 assumption is excluded.

In fitting the data it became apparent that a size effect correction was necessary above $\sim$ 50 MeV , because it was impossible to fit the data below and above 50 MeV in a consistent way. We have used the size effect correction given by Eq.(25).

The E1 and E2 strength found in the (γ,p) and (γ,α) channels for each nuclei studied is summarized in Table 3.

Table 3

Percentage of E1 and E2 sums in the α and proton channel. E1 sum: 60 NZ/A MeV.mb. E2 sum: 0.22 $Z^2A^{-1/3}$ μb/MeV.

Nucleus	Decay Channel	E1	E2
^{56}Fe	γ,α γ,p	6 ± 1 82 ± 19	7 ± 1 37 ± 15
^{59}Co	γ,α γ,p	7 ± 1 67 ± 12	5 ± 1 28 ± 11
^{64}Zn	γ,α γ,p	18 ± 4 154 ± 30	25 ± 3 77 ± 21
^{58}Ni	γ,α γ,p	4.8 ± 0.5 126 ± 12	15 ± 3
^{60}Ni	γ,α γ,p	4.4 ± 0.7 53 ± 6	15 ± 4
^{62}Ni	γ,α γ,p	2.4 ± 0.3 28 ± 2	6 ± 2

For the Ni isotopes our data went up to E_o=50 MeV and for the other targets up to 100 MeV. As a consequence we were unable to extract the E2 strength for the proton channel in the Ni isotopes. Because the E1 strength is much bigger than the E2 in the proton channel, it is necessary to go to higher incident energies in order to have enough enhancement of the E2 excitation relatively to the E1 . The E2 strength found in all cases is concentrated in the region 14-20 MeV, so it is in the region of the isoscalar E2. If we add to the (γ,p) and (γ,α) channels the neutron channel, we find that the photo cross sections integrated ut to 30 MeV exhaust ∿ 1.2 E1 sums and nearly two E1 sums when integrated up to 100 MeV. This can be compared with the results of Ahrens et al. /63/ for light elements and by Leprêtre et al. /64/ for Pb , both obtain nearly two dipole sums.

In table 4 the decay branchs of the isoscalar E2 resonance obtained from our experiments are compared with decay branches obtained in (α,α',x) coincidence experiments /65-67/ and also with the predictions

of a Hauser-Feshbach calculation /65-67/.

Table 4
Decay branches for ^{64}Zn, ^{58}Ni and ^{62}Ni

Nucleus	Channel	α,α',x	(e,x)	Calculation	Ref.
^{64}Zn	α	20 ± 4	25 ± 3	26	67
	p	38 ± 7	77 ± 21	46	67
	n	59 ± 27		28	67
^{58}Ni	α	12	15 ± 3	6	66
	p	59	-	61	66
	α	<30			65
	p	65 ± 20			65
^{62}Ni	α	<15	6 ± 2	4	65
	p	20 ± 10	-	2	65

For heavy nuclei which have fission barriers higher than the energy of the isoscalar E2 resonance the only possible decay channel for this resonance is the neutron channel, since the Coulomb barrier will prevent charged particle decays. In such nuclei, measurements of the (e,n) cross section could yield useful information about the E2 isoscalar resonance. It would also be interesting to look for the isovector E2 resonance in the 2n or 3n decay channel.

The (e,n) cross section for ^{197}Au is being measured in São Paulo and the preliminary results are shown in Fig. 32. The cross section represented by the open circles was obtained by counting directly the neutrons /68/ and that represented by the full circles was measured by radioactivity /69/. The points on the curve labelled (e+γ) were obtained interposing a 0.717 g/cm^2 Cu radiator in the beam, ahead of the target. The curve labelled E1 results from integrating the (γ,n) cross section measured at Saclay /70/ with the E1 spectrum and the curve (e+γ) is the corresponding yield of photo plus electrodisintegration. Our photodisintegration data shows good agreement with the calculated values, but the measured electrodisintegration is bigger than what expected for pure E1, indicating the existence of other multipole components. Assuming the other multipole component to be E2 and representing the E1 and E2 components by histograms, the results of the fit are shown in Fig. 33. The smooth curves through the data points result from combining the histograms, representing the E1 and E2 (γ,n) cross sections in eq.(2) and (39) with the E1 and E2 virtual photon spectra. The integrated (γ,n) cross section obtained from the fit shown in Fig. 33 is 2184 ± 195 MeV.mb. This value is

in good agreement with measurements of (γ,n) cross section. The integrated (γ,n) cross section is 2190 MeV.mb for the Livermore data /71/ and 2588 MeV.mb for the Saclay data /70/. However, the E2 strenght derived from our experiment is 210 ± 35 percent of the E2 sum.

The measurement of the (e,n) cross section by counting directly the neutrons was performed two years ago. Because we needed about two E2 sums to explain our results we repeated the measurement of the (e,n) cross section, using residual activity. The results of both measurements are in good agreement as shown in Fig. 32. Since both experiments are independent we believe the large amount of E2 found is not caused by an instrumental error.

^{197}Au has been studied in an (e,e') experiment by Pithan et al. /72/. They found an E2 resonance at 10.8 MeV excitation energy exhausting 77 percent of the E2 sum. However, more strength is observed below 10 MeV. A resonance at the excitation energy of 9.2 MeV was identified as E0, but it could be also E2, since the experiment does not discriminate between E0 and E2. In the (e,n) experiment we cannot excite E0 because of the low bombarding energies used.

The conclusion that can be derived at this point from the (e,n) experiment is that there is either about two E2 sums in the absorption cross section or there is another multipole besides E2 and E1. The other multipole that could easily be excited at these bombarding energies is M1. It would be interesting to study ^{197}Au in a more detailed (e,e') experiment and or using other probes and, whenever possible, in a (e,e',n) coincidence experiment.

Conclusions

The virtual photon method offers an opportunity to explore nuclear excitations without the drawbacks of other approaches, like the radiative tails of inelastic electron scattering or the backgrounds encountered in hadron scattering experiments.

We need more experimental results to test the regions of validity of the theory for E1 and E2 multipoles and to test the size effects correction.

References

1. W.C. Barber and V.S. Vanhuyse, Nucl. Phys., 16, 381 (1960).
2. C.F. Weizsäcker, Z. Phys., 88, 56 (1934).
3. E.S. Williams, Phys. Rev. 45, 729 (1934).
4. C.G. Wick, Ricerca Sci., 11, 49 (1940).
5. J.A. Thie, C.J. Mullin and E. Guth, Phys. Rev., 87, 962 (1952).
6. R.H. Dalitz and D.R. Yennie, Phys. Rev., 105, 1598 (1957).

7. K. Alder, A. Bohr, T. Huus, B. Mattelson, and A. Winter, Rev. Mod. Phys., 28, 432 (1956).
8. W.C. Barber, Ann. Rev. Nucl. Sci., 12, 1 (1962).
9. T. de Forest and J.D. Walecka, Advances in Physics, 15, 1 (1966).
10. G. Bishop, in Nuclear Structure and Electromagnetic Interactions, edited by N. MacDonald (Oliver and Boyd, Edinburgh, Scotland, 1964).
11. H. Uberall, Electron Scattering from Complex Nuclei (Academic Press, New York, 1971).
12. J.M. Eisenberg and W. Greiner, Excitation Mechanisms of the Nucleus (North Holland Publishing Co., Amsterdam, 1970).
13. W.C. Barber, Phys. Rev., 111, 1642 (1958).
14. W.C. Barber and T. Wiedling, Nucl. Phys., 18, 575 (1960).
15. K.L. Brown and R.W. Wilson, Phys. Rev., 93, 443 (1954).
16. M.B. Scott, A.O. Hanson and D.W. Kerst, Phys. Rev., 100, 209 (1956).
17. R.L. Hines, Phys. Rev., 105, 1534 (1957).
18. W.W. Gargaro and D.S. Onley, Phys. Rev., C4, 1032 (1971).
19. C.W. Soto Vargas, D.S. Onley and L.E. Wright, Nucl. Phys., A288, 45 (1977).
20. I.C. Nascimento, E. Wolynec and D.S. Onley, Nucl. Phys., A246, 210 (1975).
21. D.B. Isabelle and G.R. Bishop, Nucl. Phys., 45, 209 (1963).
22. E. Wolynec, W.R. Dodge, R.G. Leicht and E. Hayward, Phys. Rev., C22, 1012 (1980); and W.R. Dodge, private communication.
23. E. Hayward, in Proceedings of the Giant Multipole Resonance Topical Conference, Edited by F.E. Bertrand, Oak Ridge, Tennessee, USA, 1979, p. 275.
24. A.C. Shotter, J. of Phys., G5, 371 (1979).
25. R.H. Helm, Phys. Rev., 104, 1446 (1956).
26. M. Rosen, R. Raphael and H. Uberall, Phys. Rev., 163, 927 (1967).
27. D.F. Herring, I.C. Nascimento, R.B. Walton and R.E. Sund, Phys. Rev., 139, 562 (1965).
28. G. Kuhl and U. Kneissl, Nucl. Phys., A195, 559 (1972).
29. U. Kneissl, G. Kuhl and A. Weller, Phys. Lett., 49B, 440 (1974).
30. E. Wolynec, G. Moscati, J.R. Moreira, O.D. Gonçalves and M.N. Martins, Phys. Rev., C11, 1083 (1975).
31. E. Wolynec, G. Moscati, O.D. Gonçalves and M.N. Martins, Nucl. Phys., A244, 205 (1975).
32. M.N. Martins, E. Wolynec and G. Moscati, Phys. Rev., C16, 613 (1977).
33. U. Kneissl, G. Kuhl, K.H. Leister and A. Weller, Nucl. Phys., A256, 11 (1976).

34. A. Veyssière, H. Beil, R. Bergere, P. Carlos and A. Lepretre, Nucl. Phys., A199, 45 (1973).
35. P.A. Dickey and P. Axel, Phys. Rev. Lett., 35, 501 (1975).
36. M. Hasinoff, G.A. Fisher and S.S. Hanna, Nucl. Phys., A216, 221 (1973).
37. E. Obst, F. Rauch and E. Rosle, Phys. Rev. Lett., 21, 50 (1966).
38. K. Shoda, M. Sugawara, T. Saito and H. Miyase, Nucl. Phys., A221, 125 (1974).
39. G.B. Collins, B. Waldman and E. Guth, Phys. Rev., 55, 412 (1939).
40. G.B. Collins, B. Waldman and F. Guth, Phys. Rev., 56, 876 (1939).
41. V.J. Vanhuyse and W.C. Barber, Nucl. Phys, 26, 233 (1961).
42. W.R. Dodge and W.C. Barber, Phys. Rev., 127, 1746 (1962).
43. R.M. Hutcheon, Rep. SAL-8. Saskatchewan Accelerator Lab., Saskatoon, Sask., November 1967.
44. A.V. Vysotskaya and N.G. Afanasyev, Sov. J. Nucl. Phys., 11, 523 (1970).
45. C.F. Wong, Rept. SAL-14, Saskatchewan Accelerator Lab., Saskatoon, Saskatchewan, 1970.
46. K. Shoda, A. Suzuki, M. Sugawara, T. Saito, H. Miyase, S. Oikawa and B.N. Sung, Phys. Rev., C3, 1999 (1971).
47. K. Shoda, A. Suzuki, M. Sugawara, T. Saito, H. Miyase, S. Oikawa, and B.N. Sung, Phys. Rev., C3, 2006 (1971).
48. A. Suzuki, K. Shoda, M. Sugawara, T. Saito, H. Miyase, S. Oikawa, J. Uegaki, M.N. Thompson, K.J.F. Allen, H.J. Askin and B.N. Sung, Nucl. Phys., A257, 477 (1976).
49. J.D.T. Arruda Neto, S.B. Herdade, B.S. Bhandari and I.C. Nascimento, Phys. Rev., C18, 863 (1978) and J.D.T. Arruda Neto, Ph.D. Thesis, 1977, unpublished.
50. J.D.T. Arruda Neto, S.B. Herdade and I.C. Nascimento, Nucl. Phys., A334, 297 (1980).
51. L.J. Lindgren, A. Alm and A. Sandell, Nucl. Phys., A298, 43 (1978).
52. A.C. Shotter, D. Branford, M.C. McGeorge and J.M. Reid, Nucl. Phys., A290, 55 (1977).
53. J.D.T. Arruda Neto and B.L. Berman, Nucl. Phys., A349, 483 (1980).
54. J.D.T. Arruda Neto, S.B. Herdade, B.L. Berman and I.C. Nascimento, Phys. Rev., C22, 1996 (1980).
55. J.D.T. Arruda Neto, B.L. Berman, S.B. Herdade and I.C. Nascimento, Preprint IFUSP/P-252, to be published in Phys. Rev. C (scheduled for May-1981 issue).
56. J.D.T. Arruda Neto, S.B. Herdade, B.S. Bhandari and I.C. Nascimento, Phys. Rev., C14, 1499 (1976).
57. J.D.T. Arruda Neto, B.L. Berman, S.B. Herdade and I.C. Nascimento, Lett. Nuovo Cim., 26, 487 (1979).

58. J. van der Plicht, M.N. Harakeh, A. van der Woude, P. David and J. Debrus, Phys. Rev. Lett., 39, 1188 (1977).
59. F.E. Bertrand, J.R. Beene, C.E. Bemis Jr., E.E. Gross, D.J. Horen, J.R. Wu and W.P. Jones, Phys. Lett., 99B, 213 (1981).
60. A.C. Shotter, C.K. Gelbre, T.C. Awes, B.B. Back, J. Mahoney, T. J.M. Symmons and D.K. Scott, Phys. Rev. Lett., 43, 569 (1979).
61. J.D.T. Arruda Neto, J.R. Calarco, K. Griffioen, S.S. Hanna, D.H. H. Hoffmann, R.E. Rand, K. Wienhard and M.R. Yearian, private communication.
62. J.L. Mathews and R.O. Owens, Nucl. Instrum. Methods, 111, 157 (1973).
63. J. Ahrens, H. Borchet, K.H. Czock, H.B. Eppler, H. Gimm, H. Gundrum, M. Kröning, P. Riehn, G. Sita Ram, A. Ziegler and B. Ziegler, Nucl. Phys., A251, 479 (1975).
64. A. Leprêtre, H. Beil, R. Bergere, P. Carlos, J. Fagot, A. Vessière, J. Ahrens, P. Axel and U. Kneissl, Phys. Lett., 79B, 43 (1978).
65. K.T. Knöpfle, Lecture Notes in Physics, 108, 311 (1979).
66. M.T. Collins, C.C. Chang, S.L. Tabor, G.J. Wagner and J.R. Wu, Phys. Rev. Lett., 42,z1440 (1979).
67. M.T. Collins, C.C. Chang, S.L. Tabor, Phys. Rev. C, to be published.
68. P. Gouffon, M.Sc. Thesis (1979) unpublished.
69. M.C.A. Campos, private communication.
70. A. Veyssière, H. Beil, R. Bergère, P. Carlos and A. Leprêtre, Nucl. Phys., A159, 561 (1970).
71. S.C. Fultz, R.L. Bramnlett, J.T. Caldwell and N.A. Kerr, Phys. Rev., 127, 1273.
72. R. Pittham, F.R. Buskirk, E.B. Daley, J.N. Dyer and X.K. Maruyama, Phys. Rev. Lett. 33, 849 (1974).

Figure Captions

Fig. 1 - El and E2 virtual photon spectra for 10 MeV electrons scattered from a uranium nucleus, calculated in distorted wave and in plane wave (PW) Born approximation.

Fig. 2 - The DWBA virtual photon spectra for 27 MeV electrons and positrons scattered by targets of various Z .

Fig. 3 - The ratio of the number of 16.6 MeV longitudinal to transverse photons in DWBA El and E2 spectra as a function of E_o .

Fig. 4 - Isochromates for an El transition of energy 10 MeV. The full curves refer to values of N^{El} for a point nucleus while the broken curves refer to values of N^{El} for nuclei with mass number A=10 to 240. Transverse and longitudinal components are labelled by T and L .

Fig. 5 - Isochromates for an E2 transition of energy 10 MeV. The full curves refer to values of N^{E2} for a point nucleus while the broken curves refer to values of A=10 to 240. Transverse and longitudinal components are labelled by T and L .

Fig. 6 - El and E2 size effect correction for an excitation energy of 10 MeV versus the electron incident energy.

Fig. 7 - The ratio of cross sections produced by 27.5 MeV electrons and positrons as a function of Z .

Fig. 8 - The ratio of cross sections produced by electrons and positrons for the fission channel in ^{232}Th as a function of electron and positron incident energy.

Fig. 9 - The ratio of measured to predicted cross section for the neutron channel in ^{238}U .

Fig. 10 - Proton spectrum at 90^{o} for ^{90}Zr and incident electrons of 60 MeV.

Fig. 11 - Proton spectrum in the region of the 16.3 MeV analogue state in ^{90}Zr .

Fig. 12 - Radiation width Γ versus the electron incident energy. a) without size effect correction; b) with size effect correction. The dashed lines show the value of $\bar{\Gamma}$ obtained from photoexcitation.

Fig. 13 - E1 and E2 virtual photon spectra for 25 MeV electrons scattered from a uranium nucleus.

Fig. 14 - Proton spectra for ^{181}Ta at various electron incident energies E_e .

Fig. 15 - Electrodisintegration cross section for protons emitted at 90 degrees from ^{181}Ta as a function of electron indicent energy E_o .

Fig. 16 - Photodisintegration cross section for ^{181}Ta versus the photon energy E , derived assuming pure E1 excitation.

Fig. 17 - Angular distribution of protons from ^{181}Ta having energies in the region of the second peak

Fig. 18 - E1 , E2 and E3 virtual photon spectra generated when a 50 MeV electron scatters from a Ni nucleus.

Fig. 19 - Functions that fit measured angular distributions of fission fragments, produced by 6 MeV electrons (e,f) and by bremsstrahlung of end point energy 6 MeV (γ,f).

Fig. 20 - Electrofission cross section for ^{238}U , versus the electron incident energy. The curve shows the predicted cross section for a pure E1 process.

Fig. 21 - The difference between the measured electrofission cross section and the predicted values for pure E1. The curve results from folding back the E2 cross section derived from these data points.

Fig. 22 - $\sigma^{E2}_{\gamma,f}$ obtained from the electrofission measurements.

Fig. 23 - Top: inelastic alpha spectra from the reaction $^{238}U(\alpha,\alpha',f)$ for the indicated angles. Contaminants are shown cross hatched. At 11.5^{o} , the deduced shape of the giant resonance peak and the underlying continuum are shown.

Middle: spectra of alpha particles measured in coincidence with fission fragments. In the 11.5^{o} spectrum an enhancement indicated by the smooth curve is attributed to fission decay of the $K=0$ component of the Giant Quadrupole Resonance.

Bottom: fission probability.

Fig. 24 - $^{238}U(e,e',f)$ coincidence spectrum for 80.1 MeV electrons scattered at 40 degrees.

Fig. 25 - $^{238}U(e,e',f)$ coincidence spectrum for 117.7 MeV electrons scattered at 40 degrees.

Fig. 26 - The E2 component in the fission channel derived from the (e,f) and (e,e',f) experiments.

Fig. 27 - The alpha particle spectrum at 90^{o} when 30 MeV electrons are incidente on ^{64}Zn .

Fig. 28 - The proton spectrum at 90^{o} when 30 MeV electrons are incident on ^{64}Zn .

Fig. 29 - The measured $\sigma_{e,\alpha}(E_o)$ for ^{64}Zn as a function of electron incident energy E_o (open circles). The full circles represent the yield, $Y_{e,\alpha}(E_o)$ obtained when a 0.217 g/cm^2 tantalum foil was placed in the electron beam ahead of the target. The smooth curves are the best fits to the data and were obtained by combining the histograms representing the E1 and E2 (γ,α) cross sections (right hand scale) in eq.(2) and (39) with the E1 and E2 DWBA virtual photon spectra.

Fig. 30 - The measured $\sigma_{e,p}(E_o)$ for ^{64}Zn . See caption of Fig. 29.

Fig. 31 - The result of fitting the electrodisintegration cross section of Fig. 29 with E1 only. The predicted yield for electro plus photodisintegration is much higher than the measured values (full circles).

Fig. 32 - The (e,n) cross section for ^{197}Au. The smooth curves are the predicted electrodisintegration for pure E1 and the predicted yield of electro plus photodisintegration.

Fig. 33 - The E1 and E2 (γ,n) cross sections (right hand scale) which fit the ^{197}Au (e,n) and $(e+\gamma,n)$ data.

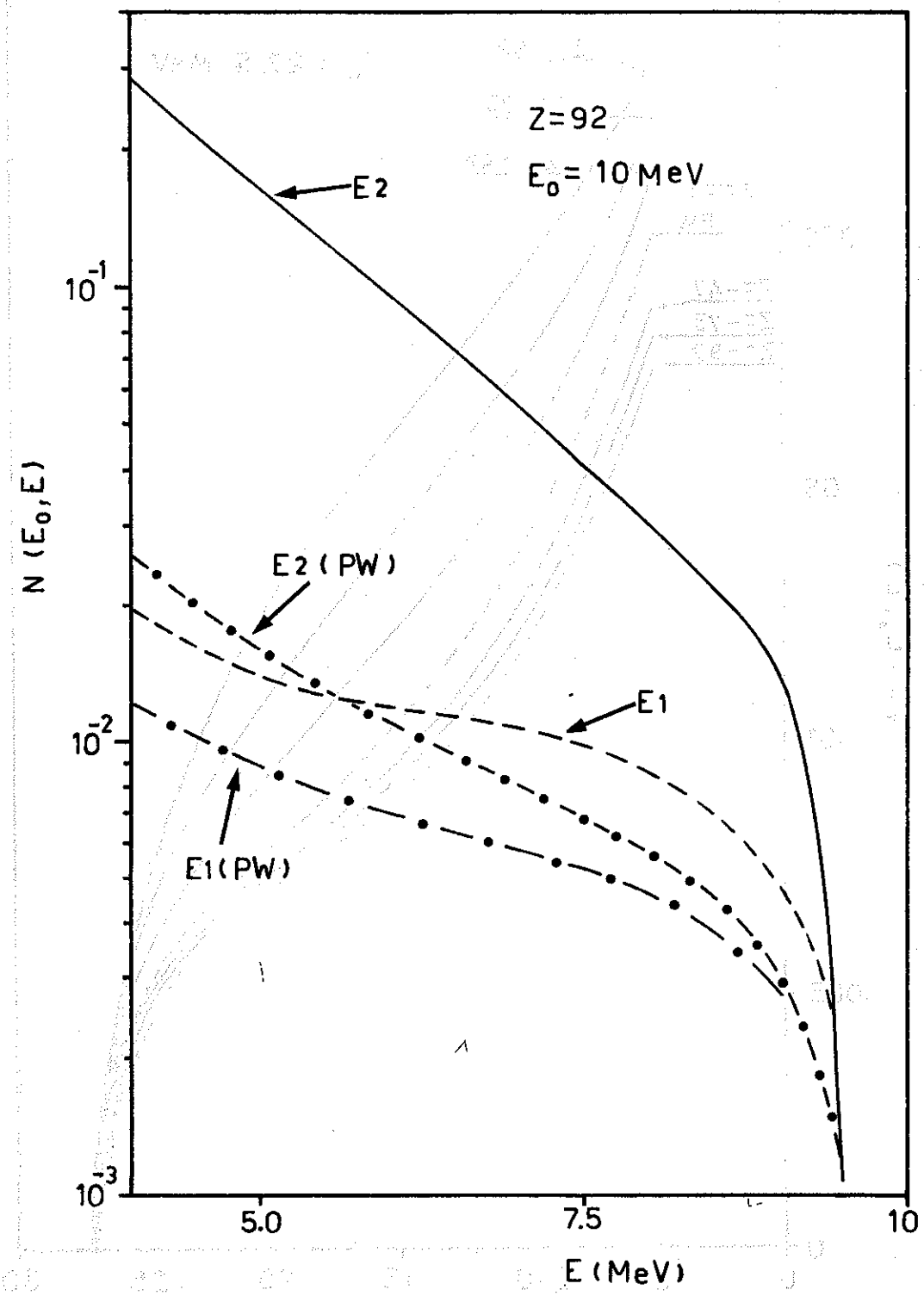

Fig.1

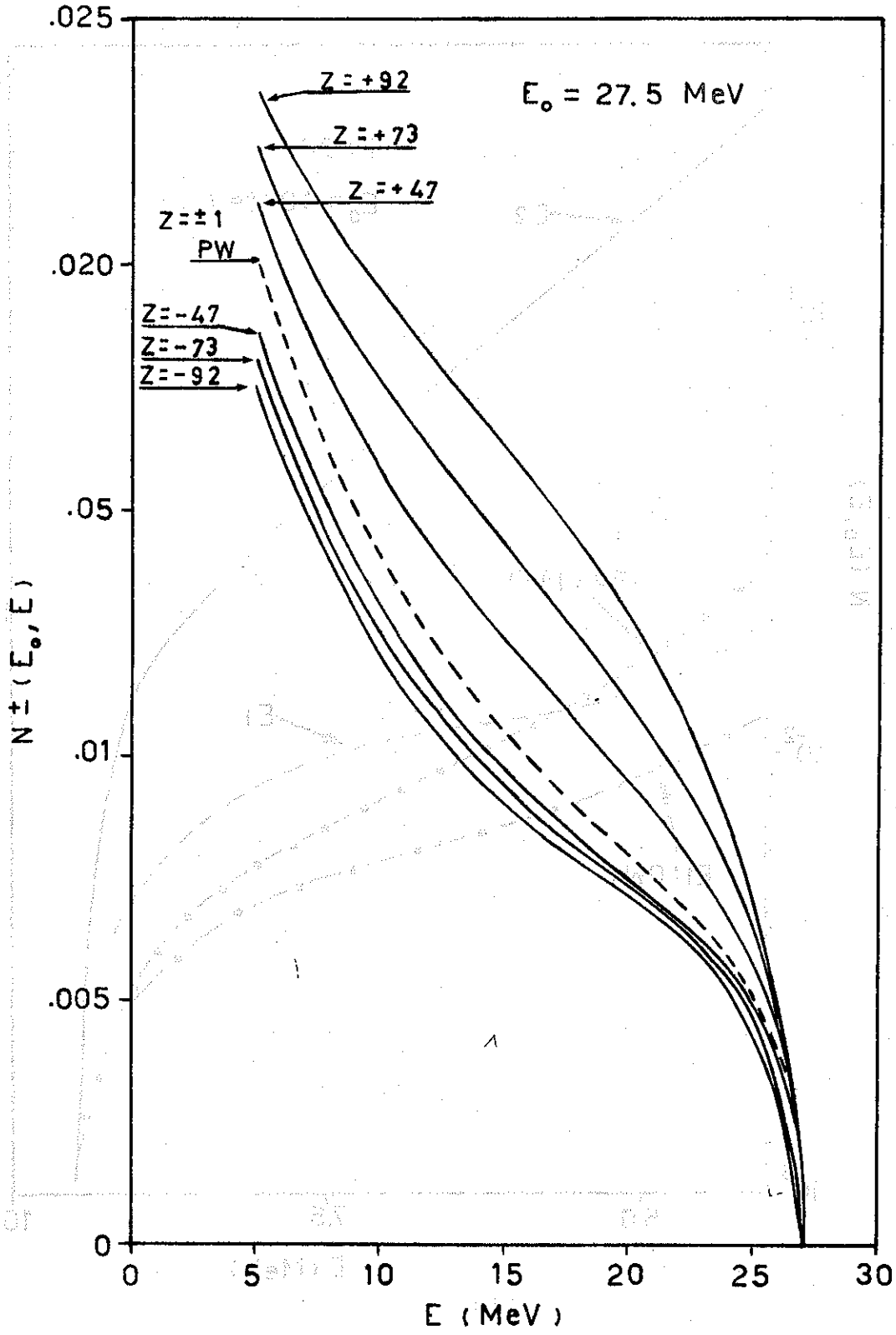
.025
.020
.05
.01
.005
0
0
5
10
15
20
25
30
E (MeV)
N± (E₀, E)
E₀ = 27.5 MeV
Z = +92
Z = +73
Z = +47
Z = ±1
PW
Z = -47
Z = -73
Z = -92

Fig.2

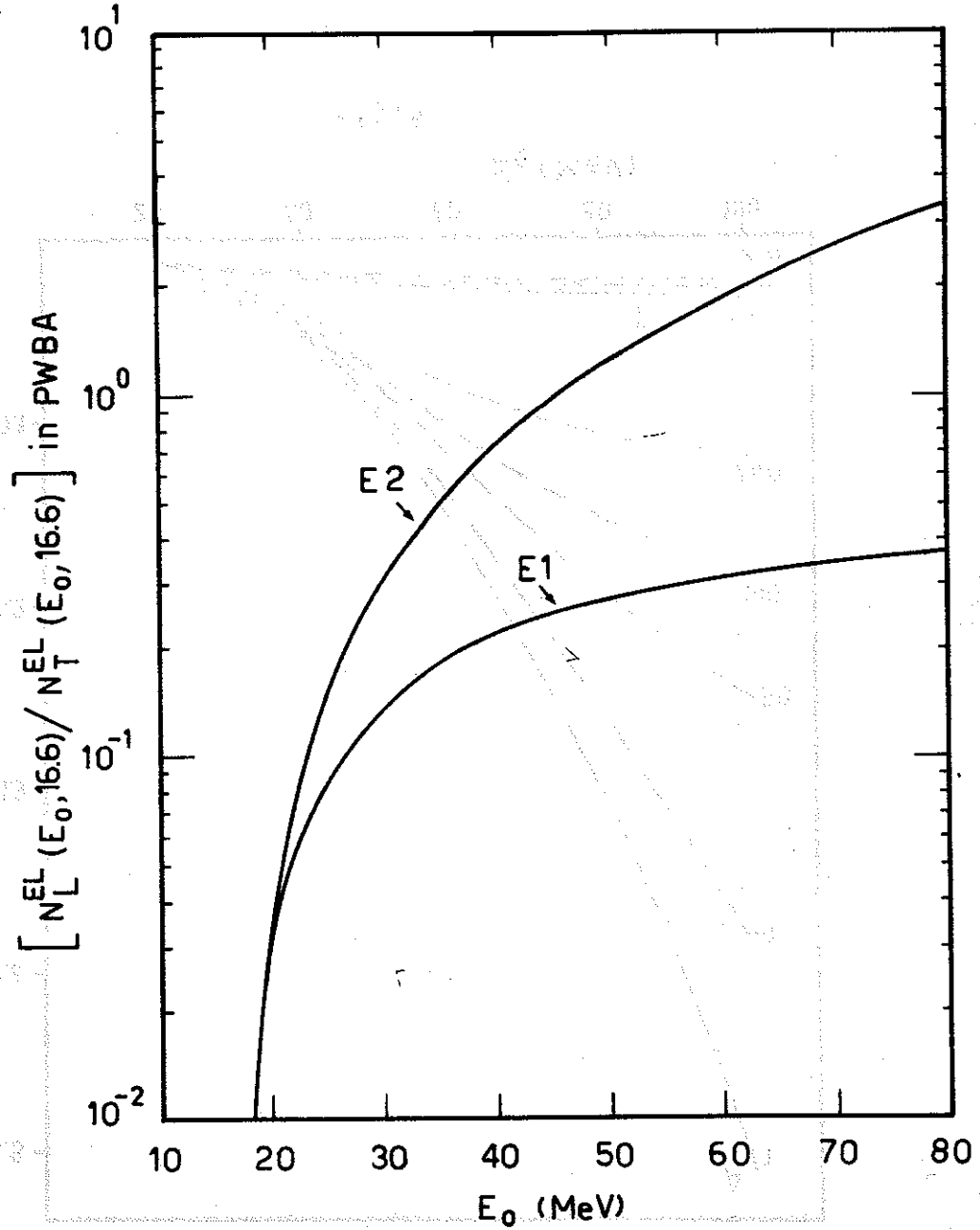
10^1
10^0
10^{-1}
10^{-2}
$\left[N_L^{EL}(E_o,16.6) / N_T^{EL}(E_o,16.6) \right]$ in PWBA
E2
E1
10
20
30
40
50
60
70
80
E_o (MeV)

Fig.3

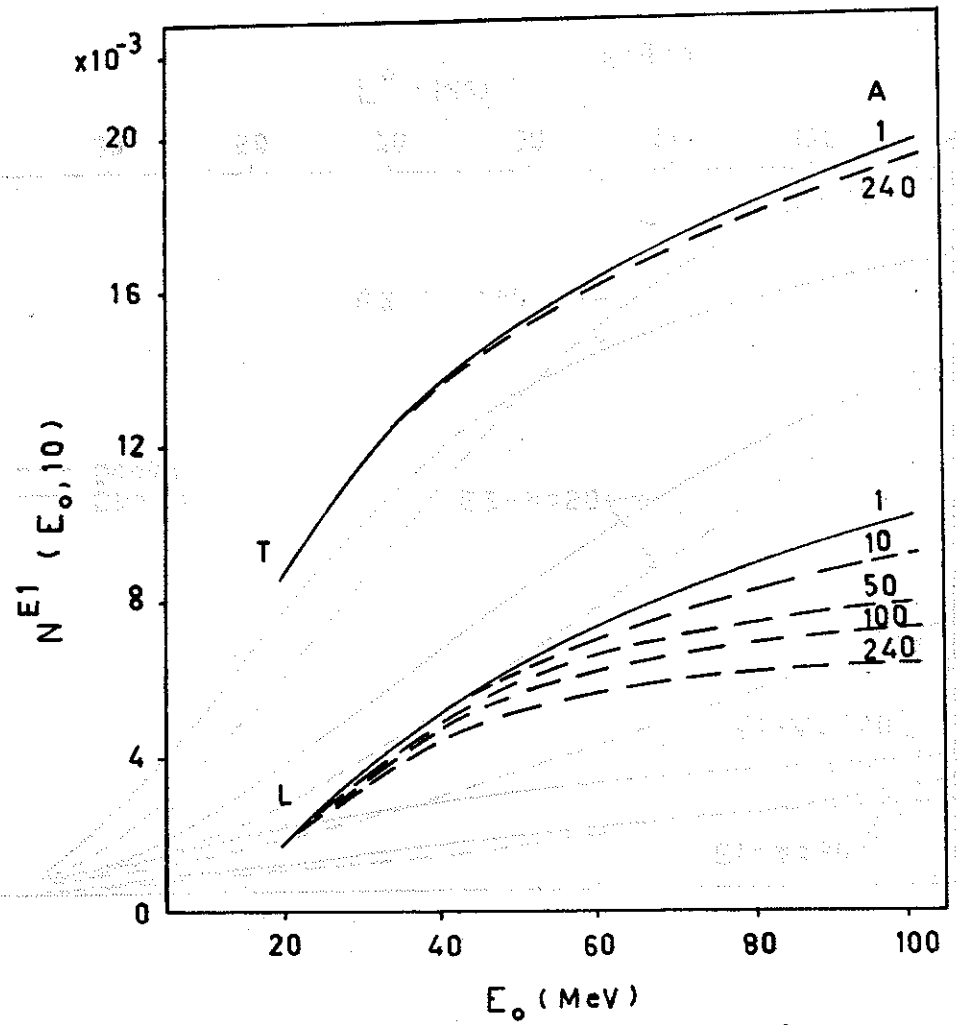
x10^{-3}
20
16
12
8
4
0
$N^{E1}(E_o,10)$
A
1
240
T
1
10
50
100
240
L
20
40
60
80
100
E_o (MeV)

Fig.4

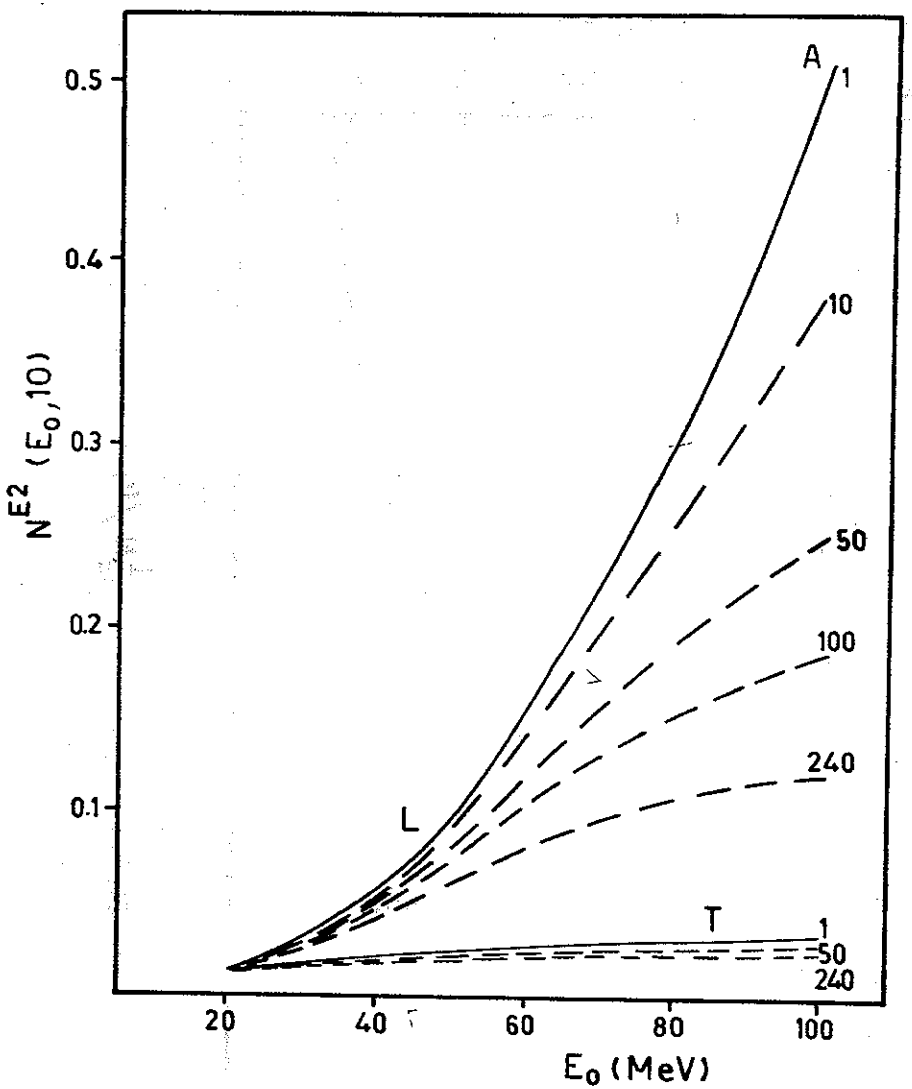
A
1
10
50
100
240
L
T
1
50
240
0.5
0.4
0.3
0.2
0.1
20
40
60
80
100
$N^{E2}(E_0,10)$
E_0 (MeV)

Fig.5

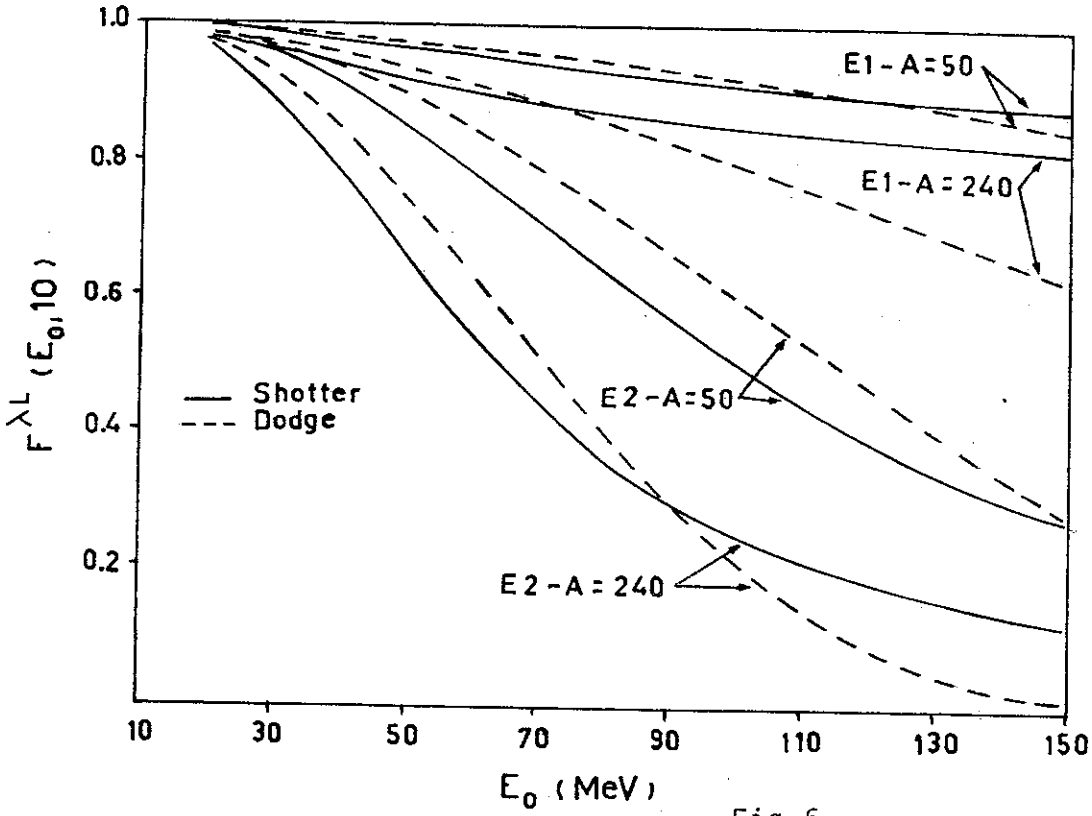
E1 - A = 50
E1 - A = 240
E2 - A = 50
E2 - A = 240
Shotter
Dodge
1.0
0.8
0.6
0.4
0.2
10
30
50
70
90
110
130
150
$F^{\lambda L}(E_0,10)$
E_0 (MeV)

Fig.6

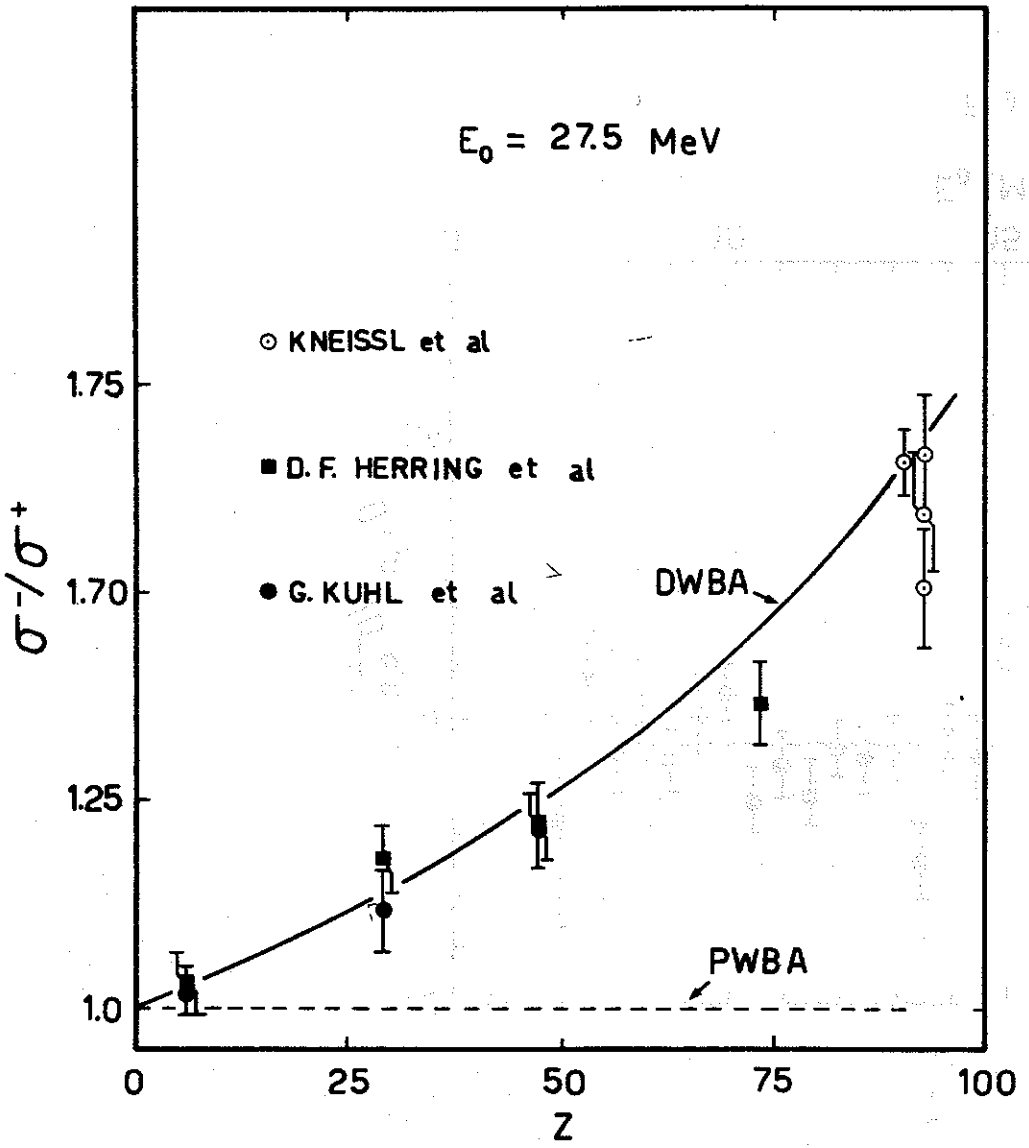
E_0 = 27.5 MeV
KNEISSL et al
D.F. HERRING et al
G. KUHL et al
DWBA
PWBA
σ^-/σ^+
1.75
1.70
1.25
1.0
0
25
50
75
100
Z

Fig.7

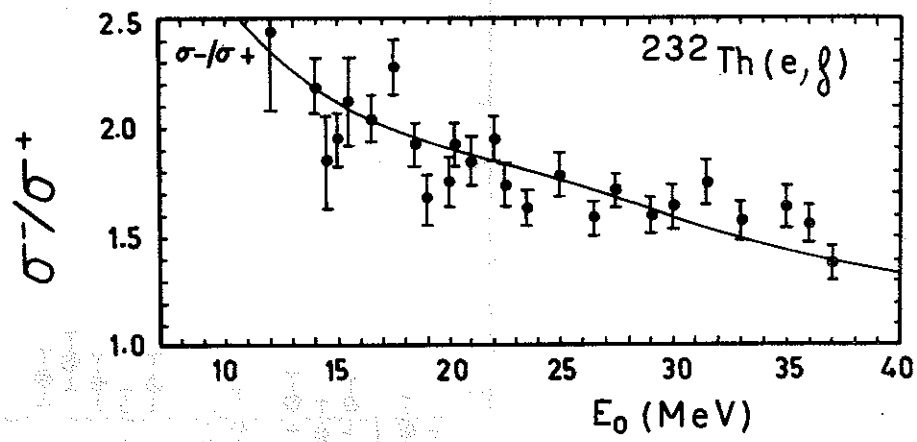
σ^-/σ^+
^{232}Th (e, g)
2.5
2.0
1.5
1.0
10
15
20
25
30
35
40
E_0 (MeV)

Fig.8

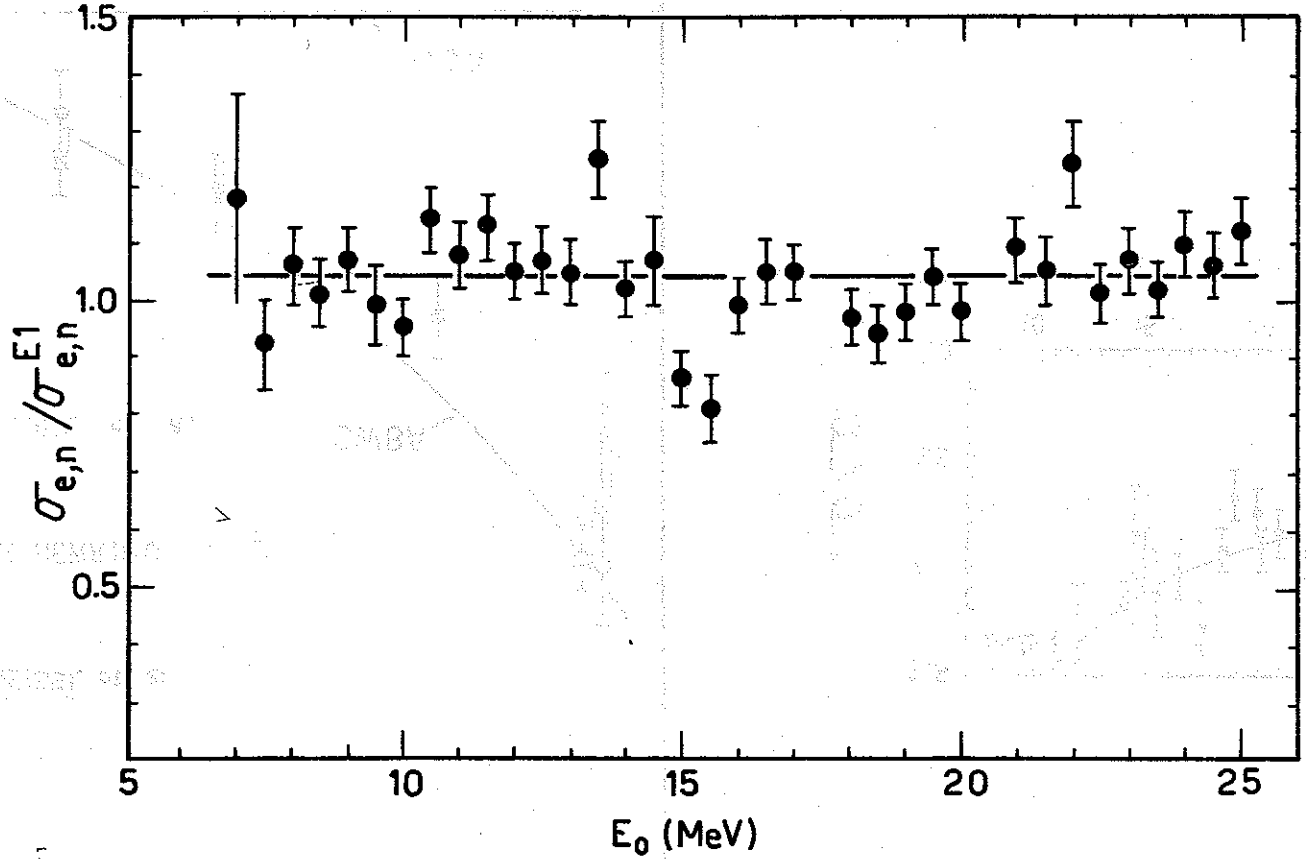

Fig.9

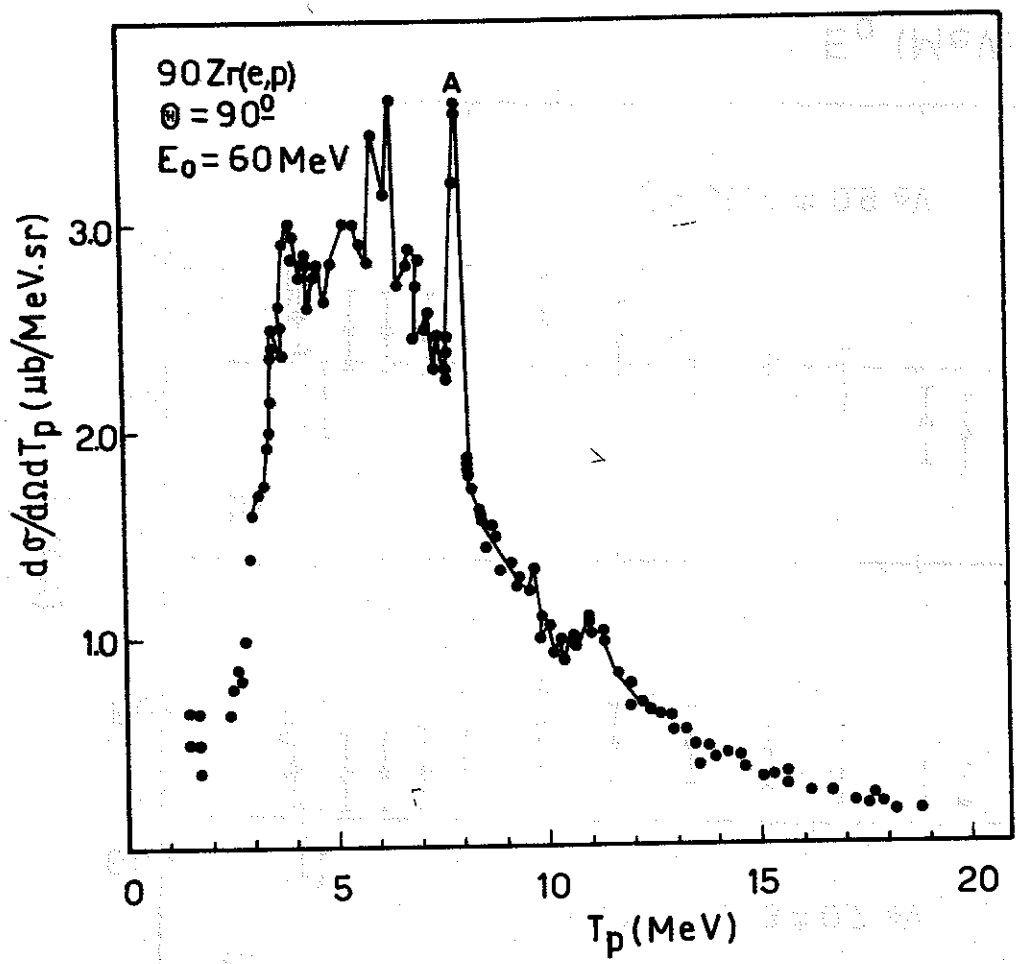
90Zr(e,p)
θ = 90°
E0 = 60 MeV
A
dσ/dΩdTp (μb/MeV.sr)
3.0
2.0
1.0
0
5
10
15
20
Tp (MeV)

Fig.10

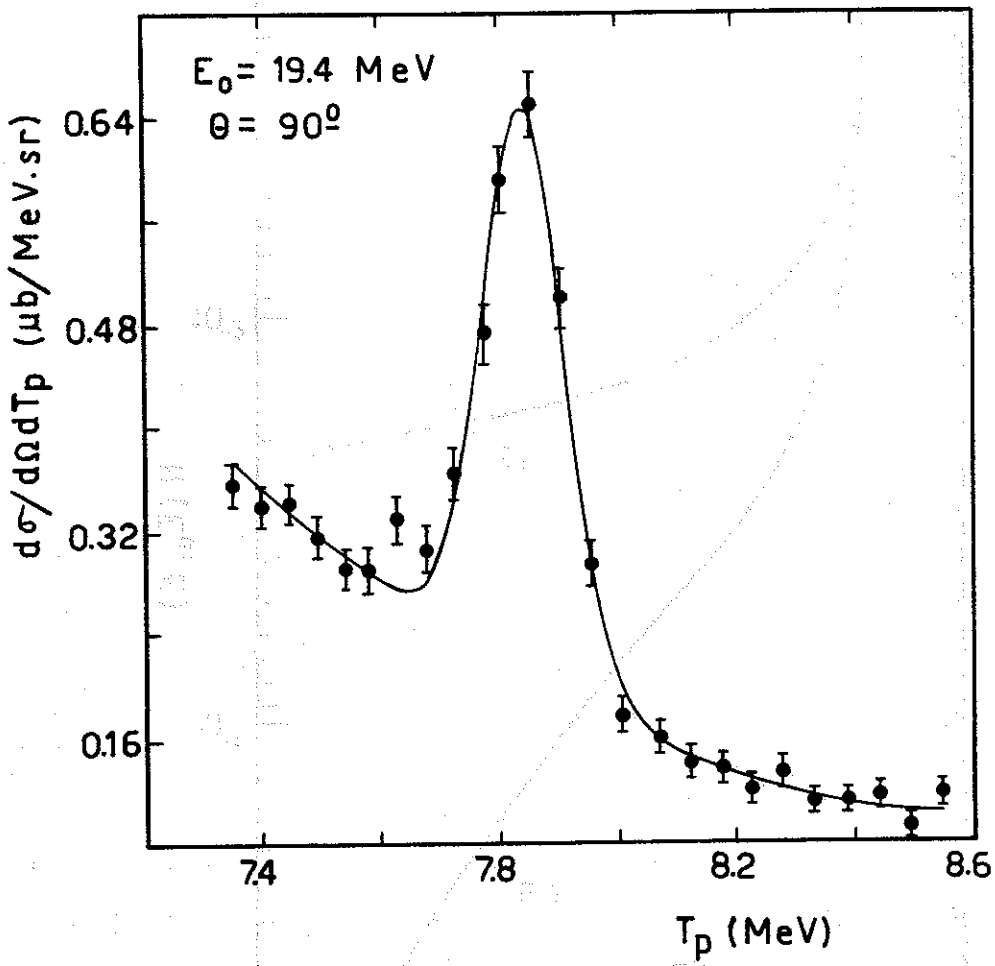
E0 = 19.4 MeV
θ = 90°
dσ/dΩdTp (μb/MeV.sr)
0.64
0.48
0.32
0.16
7.4
7.8
8.2
8.6
Tp (MeV)

Fig.11

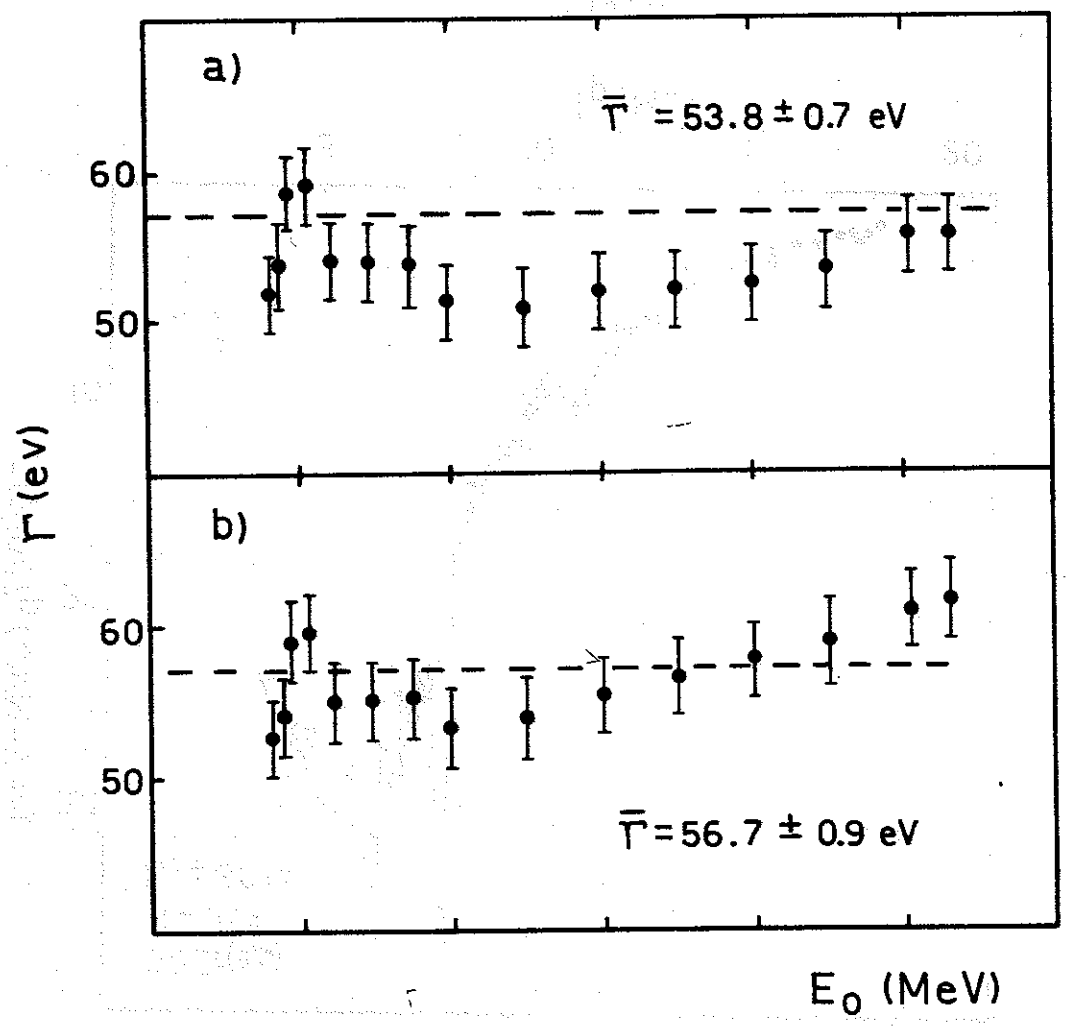
a)
$\bar{\Gamma}$ = 53.8 ± 0.7 eV
60
50
b)
60
50
$\bar{\Gamma}$ = 56.7 ± 0.9 eV
Γ (ev)
E_0 (MeV)

Fig.12

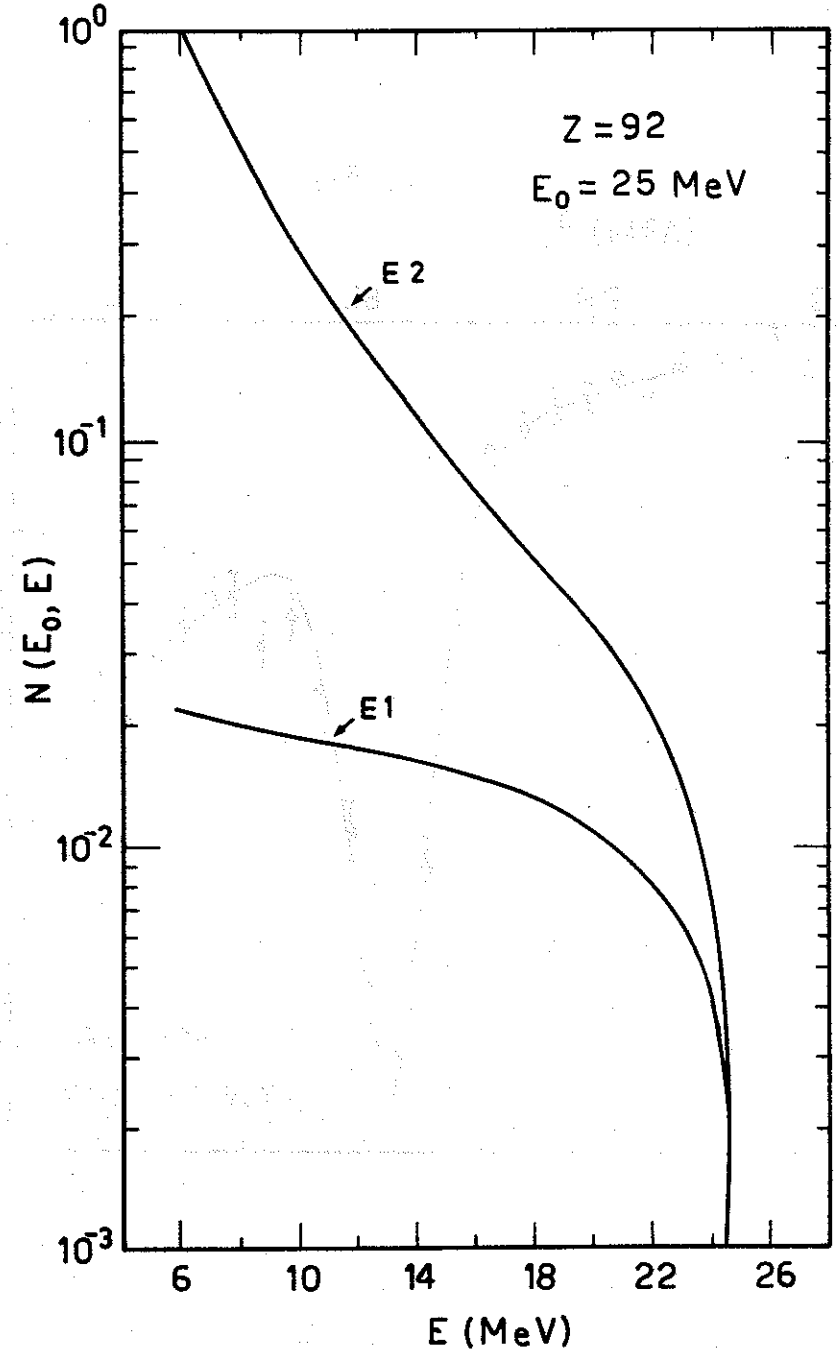
Z = 92
E_0 = 25 MeV
E 2
E1
10^0
10^{-1}
10^{-2}
10^{-3}
N (E_0, E)
6
10
14
18
22
26
E (MeV)

Fig.13

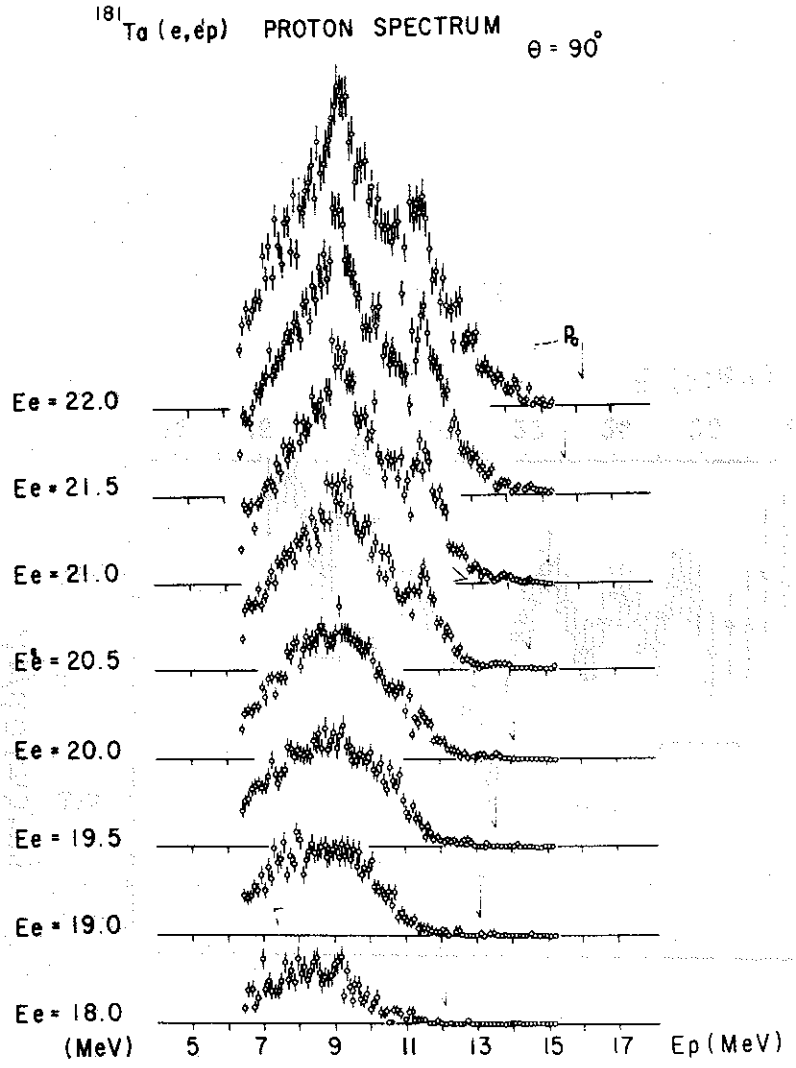
^{181}Ta (e,ep) PROTON SPECTRUM
θ = 90°
P_0
Ee = 22.0
Ee = 21.5
Ee = 21.0
Ee = 20.5
Ee = 20.0
Ee = 19.5
Ee = 19.0
Ee = 18.0
(MeV)
5
7
9
11
13
15
17
Ep (MeV)

Fig.14

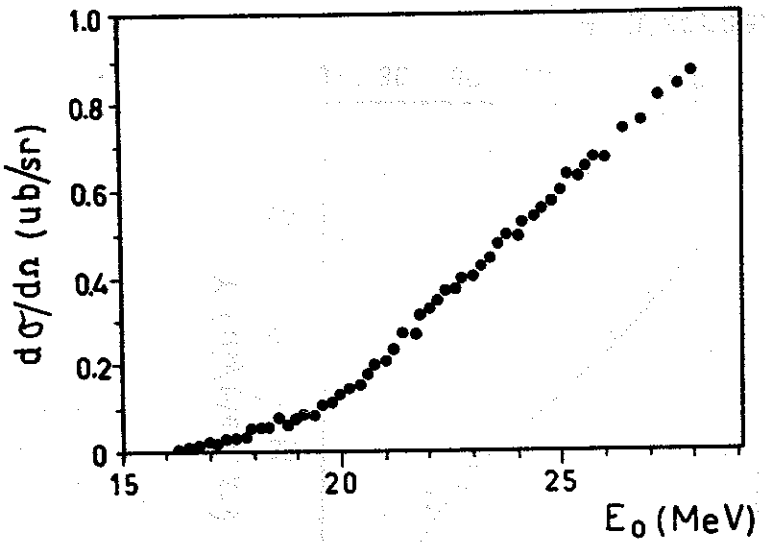
1.0
0.8
0.6
0.4
0.2
0
dσ/dΩ (ub/sr)
15
20
25
E_0 (MeV)

Fig.15

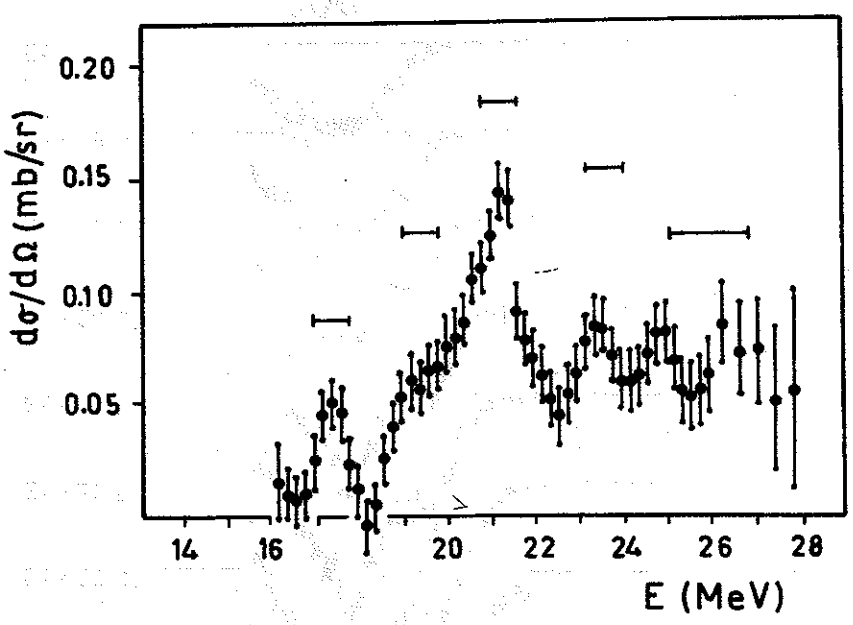
0.20
0.15
0.10
0.05
dσ/dΩ (mb/sr)
14
16
20
22
24
26
28
E (MeV)

Fig.16

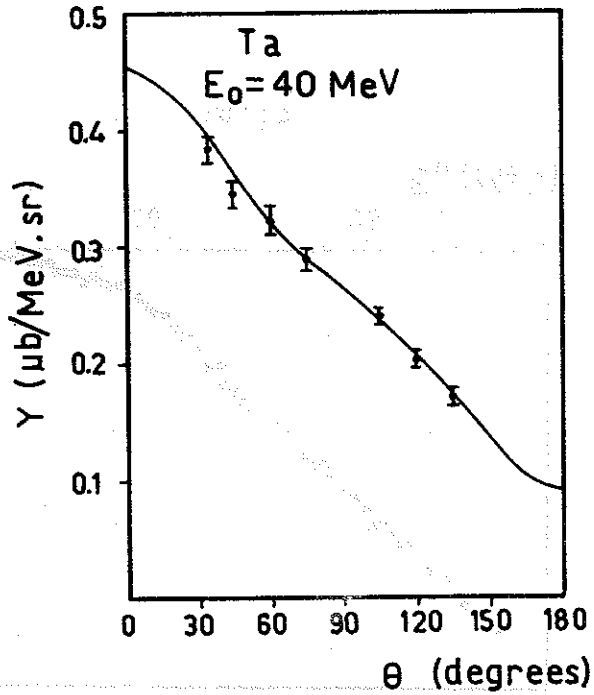
Ta
E₀= 40 MeV
0.5
0.4
0.3
0.2
0.1
Y (μb/MeV.sr)
0
30
60
90
120
150
180
θ (degrees)

Fig.17

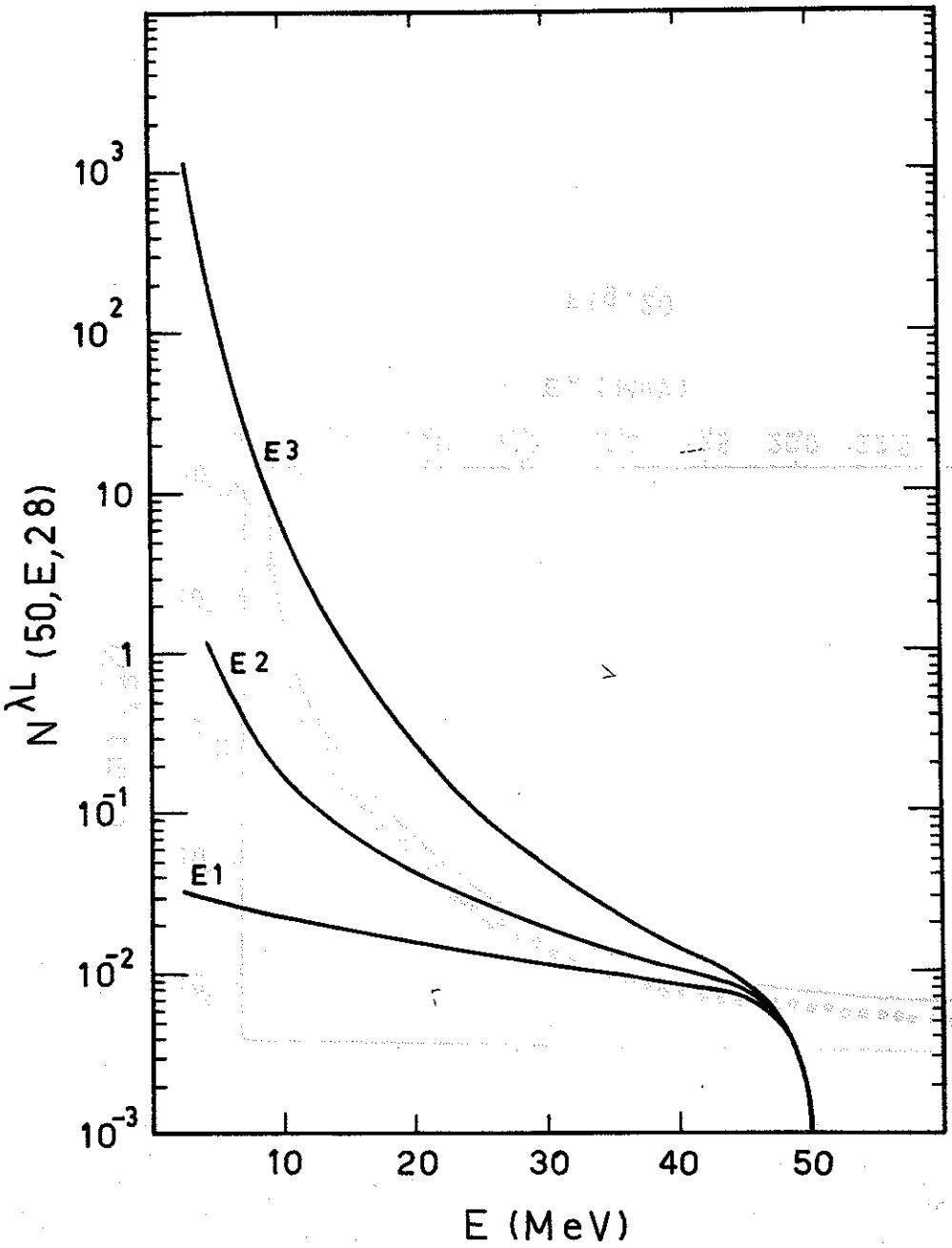
$N^{\lambda L}(50,E,28)$
10^3
10^2
10
1
10^{-1}
10^{-2}
10^{-3}
E3
E2
E1
10
20
30
40
50
E (MeV)

Fig.18

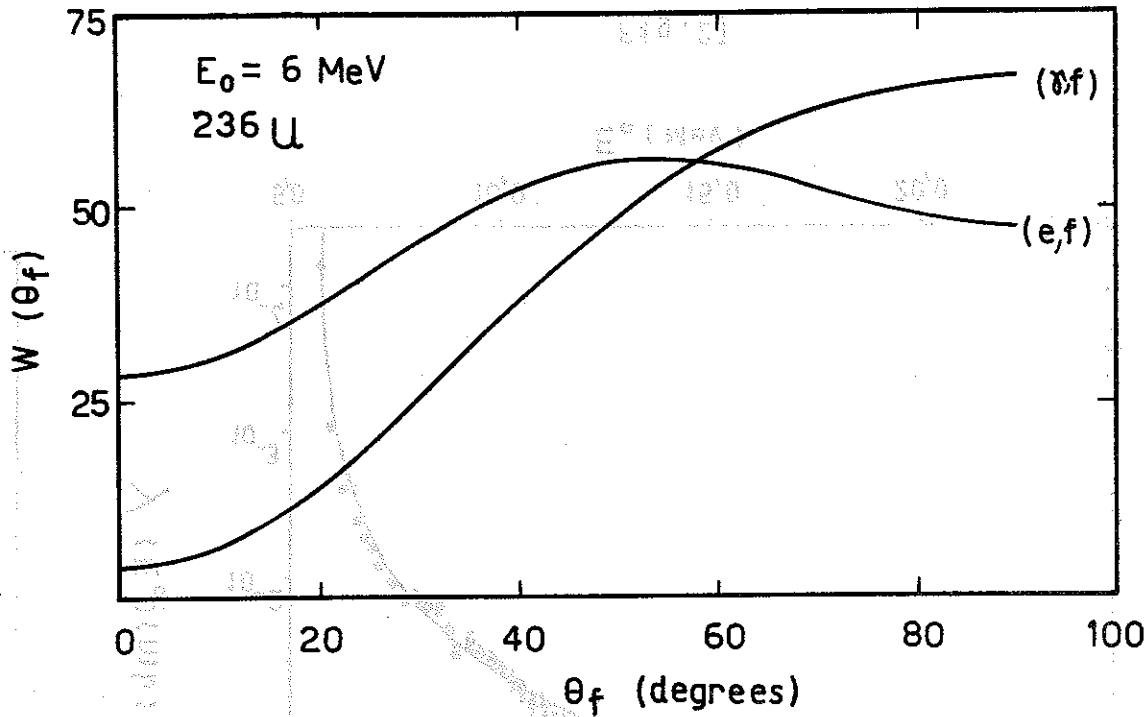
E_0 = 6 MeV
^{236}U
(γ,f)
(e,f)
W (θ_f)
75
50
25
0
20
40
60
80
100
θ_f (degrees)

Fig.19

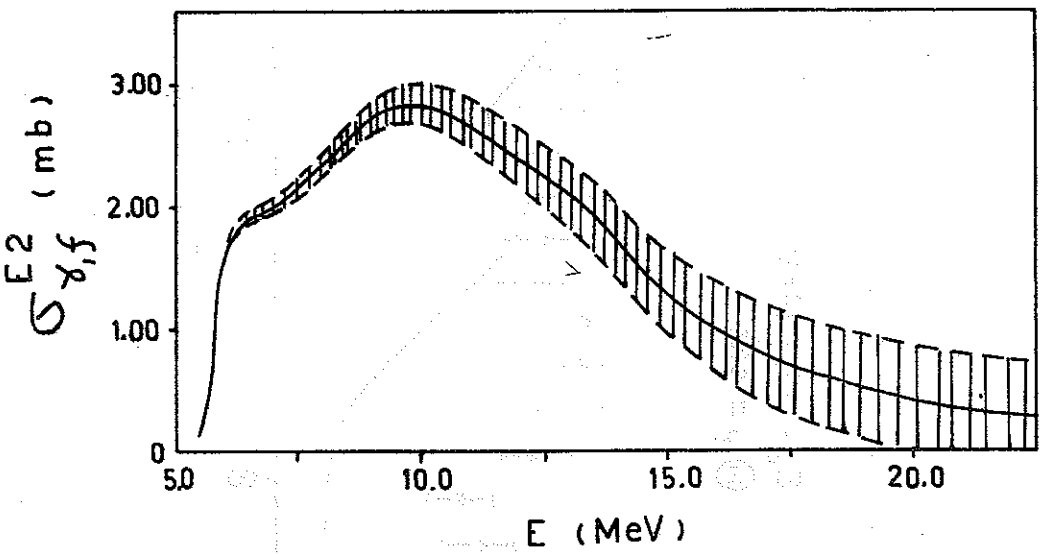
$\sigma^{E2}_{\gamma,f}$ (mb)
3.00
2.00
1.00
0
5.0
10.0
15.0
20.0
E (MeV)

Fig.22

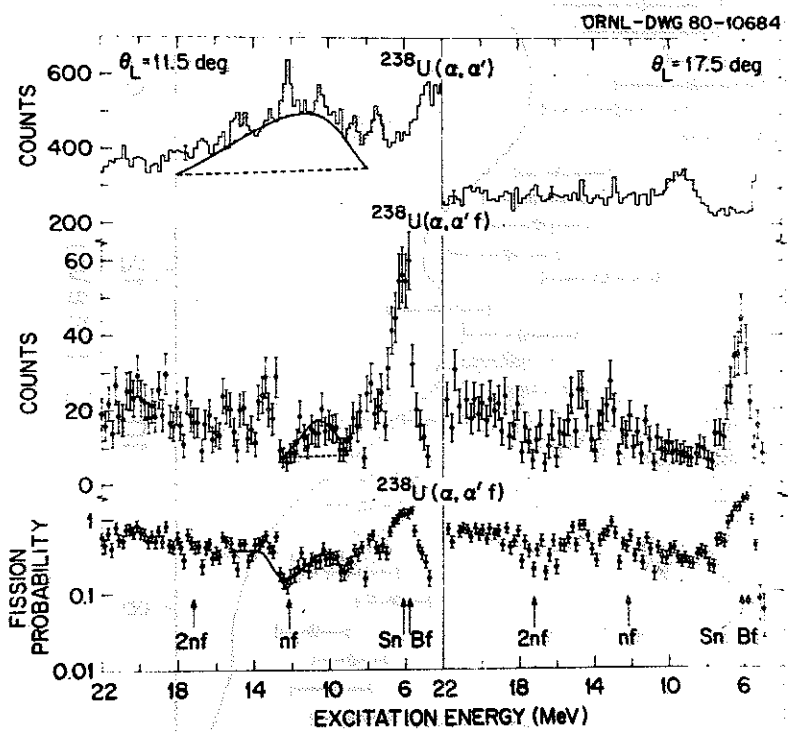
ORNL-DWG 80-10684
θ_L=11.5 deg
^{238}U(α,α')
θ_L=17.5 deg
COUNTS
600
400
200
^{238}U(α,α'f)
60
40
20
0
COUNTS
^{238}U(α,α'f)
FISSION PROBABILITY
1
0.1
0.01
2nf
nf
Sn
Bf
2nf
nf
Sn
Bf
22
18
14
10
6
22
18
14
10
6
EXCITATION ENERGY (MeV)

Fig.23

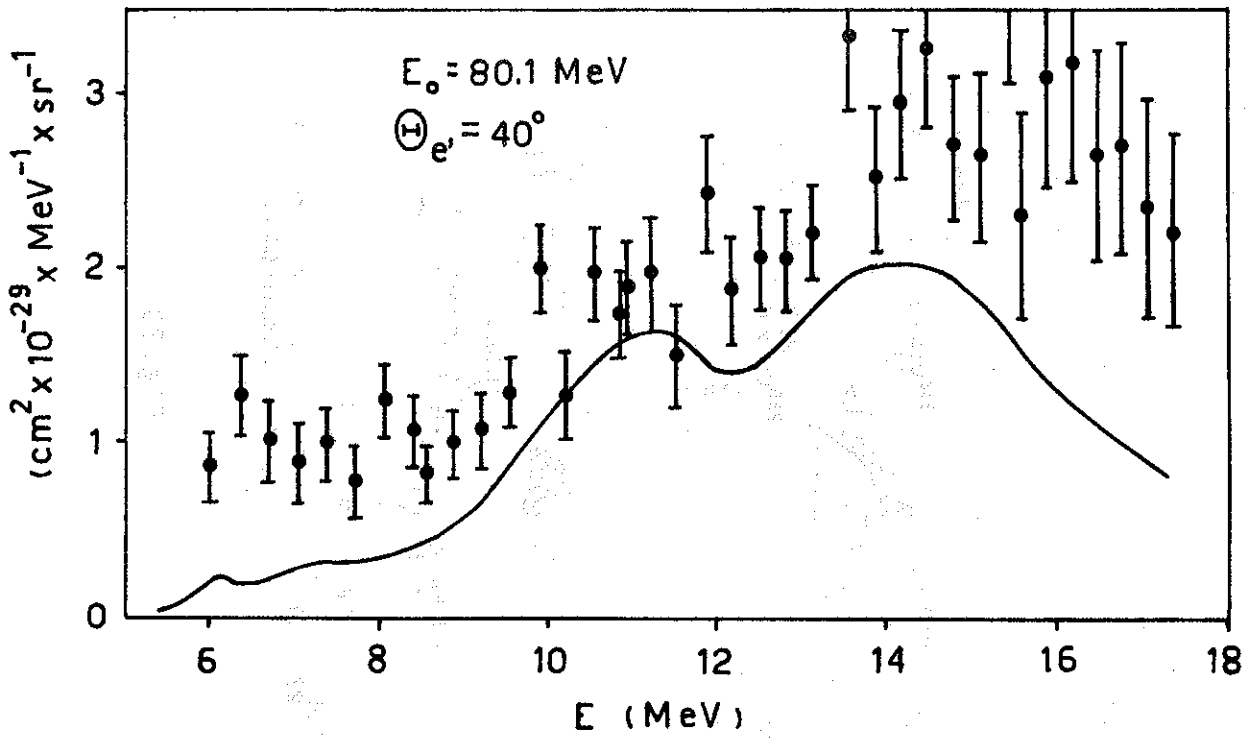
E_o = 80.1 MeV
$\Theta_{e'}$ = 40°
$(cm^2 \times 10^{-29} \times MeV^{-1} \times sr^{-1})$
E (MeV)

Fig.24

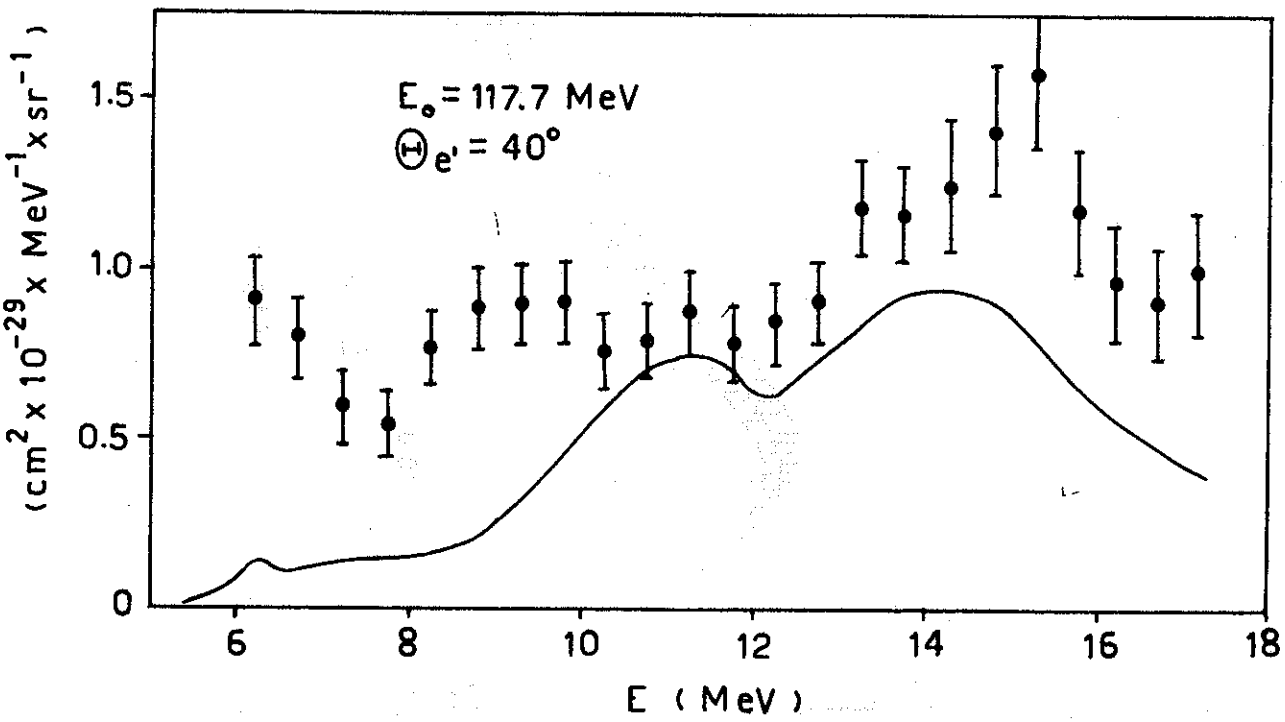
E_o = 117.7 MeV
$\Theta_{e'}$ = 40°
$(cm^2 \times 10^{-29} \times MeV^{-1} \times sr^{-1})$
E (MeV)

Fig.25

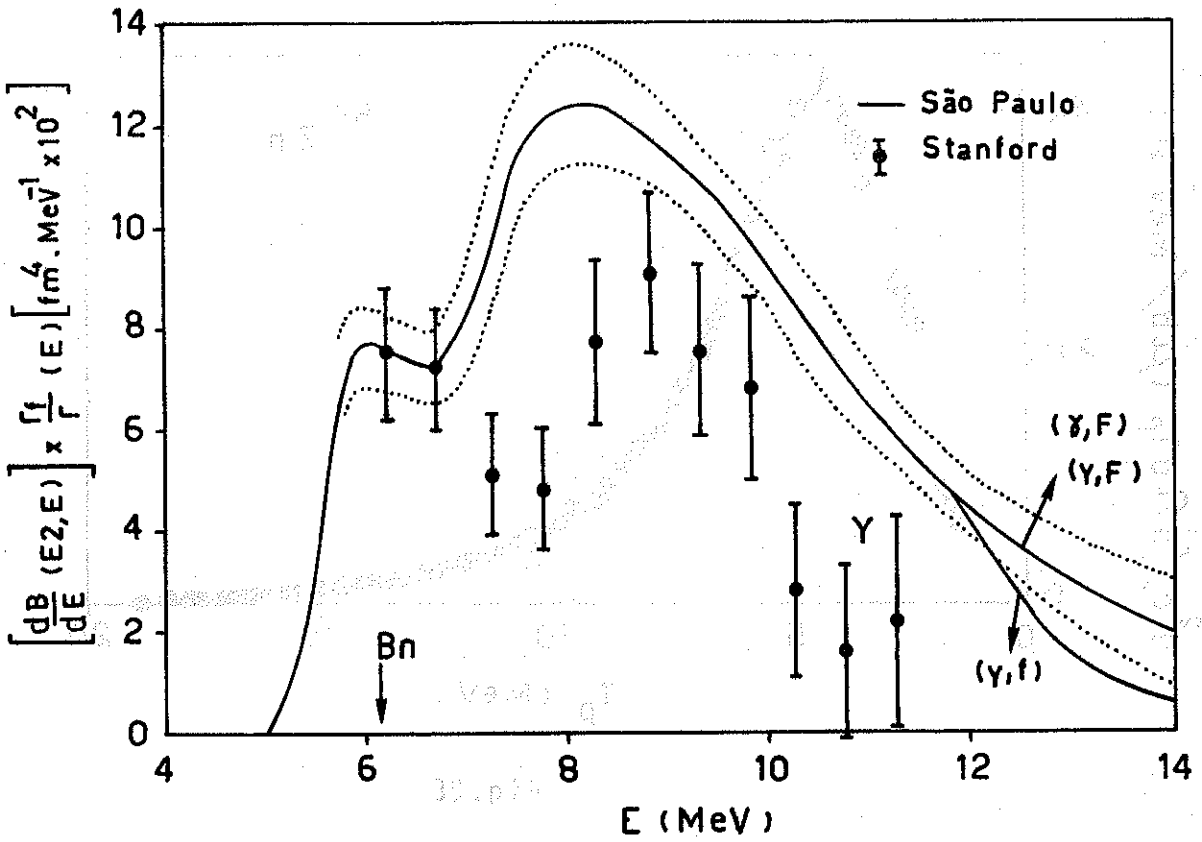

Fig.26

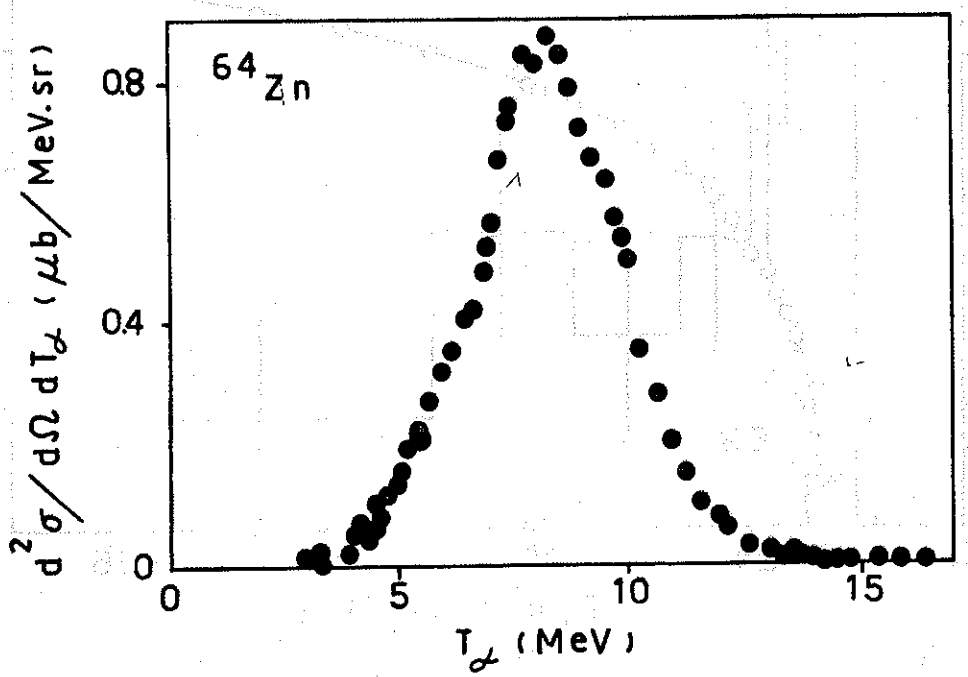

Fig.27

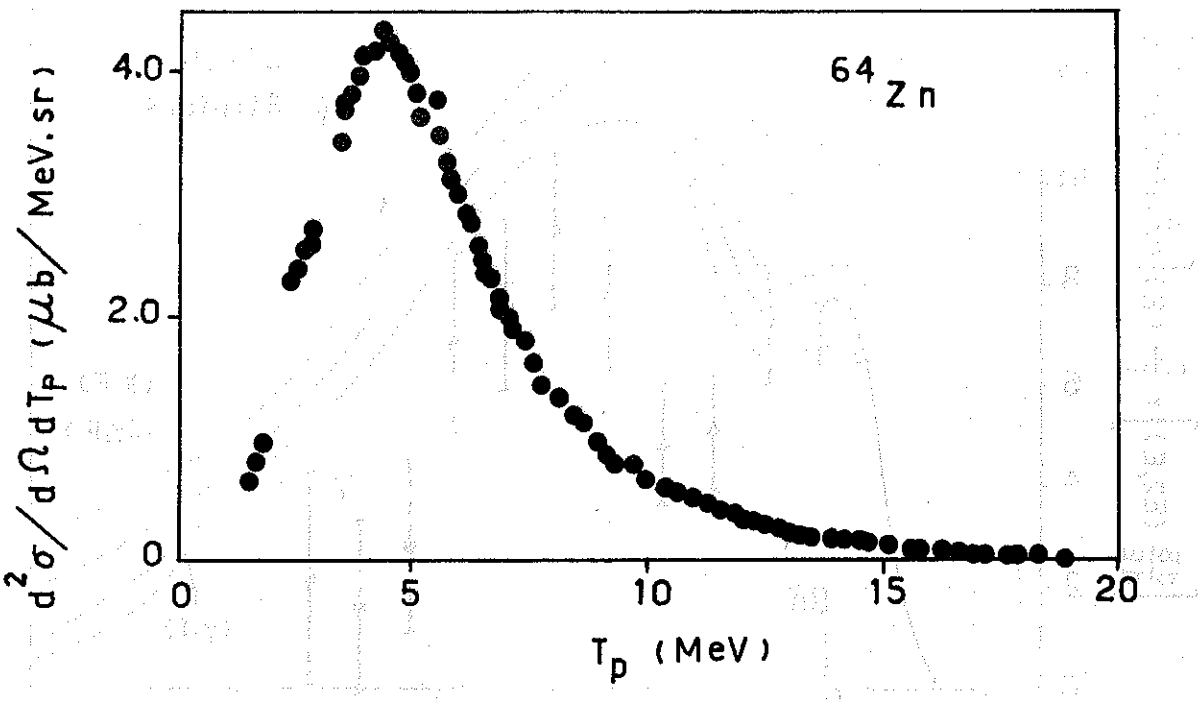
^{64}Zn
4.0
2.0
0
0
5
10
15
20
$d^2\sigma/d\Omega dT_p$ (μb/ MeV.sr)
T_p (MeV)

Fig.28

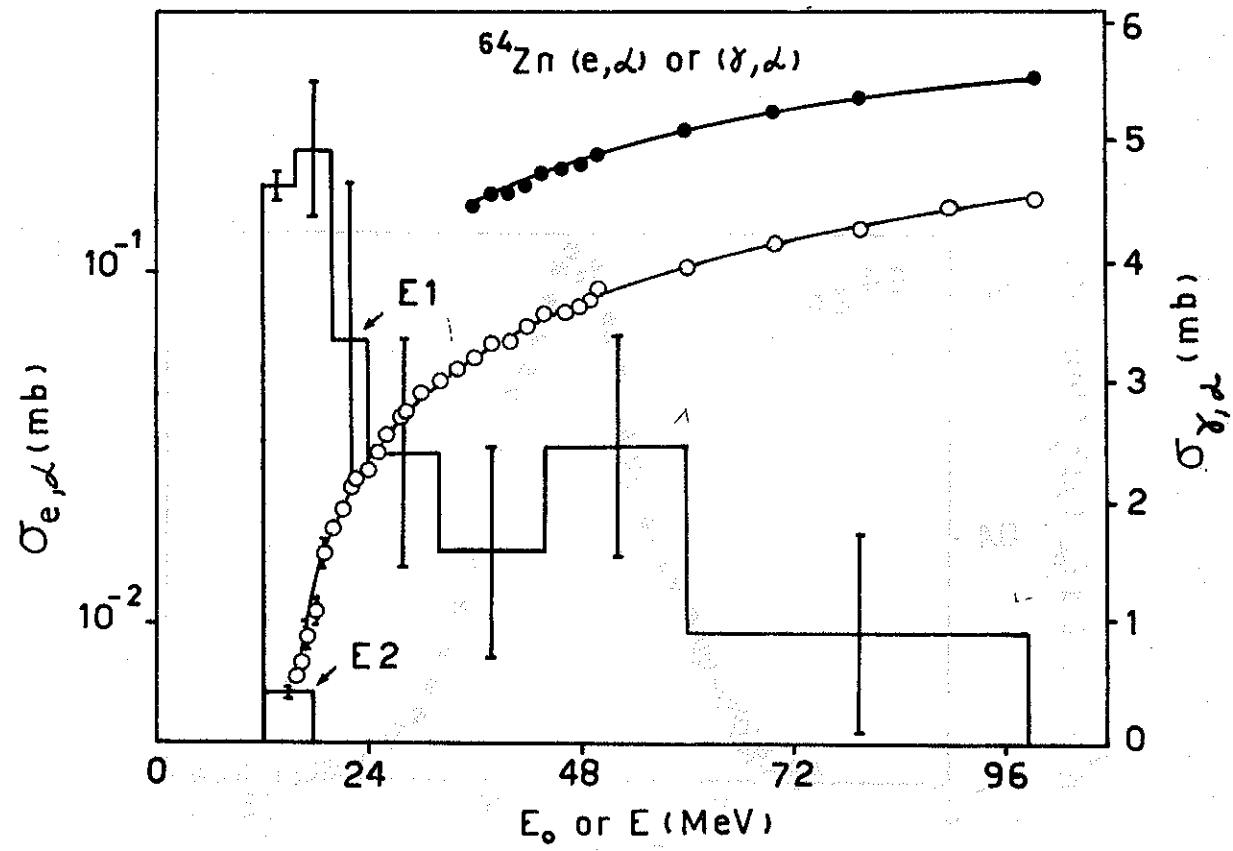
^{64}Zn (e,α) or (γ,α)
E1
E2
10^{-1}
10^{-2}
0
24
48
72
96
6
5
4
3
2
1
0
$\sigma_{e,\alpha}$ (mb)
$\sigma_{\gamma,\alpha}$ (mb)
E_o or E (MeV)

Fig.29

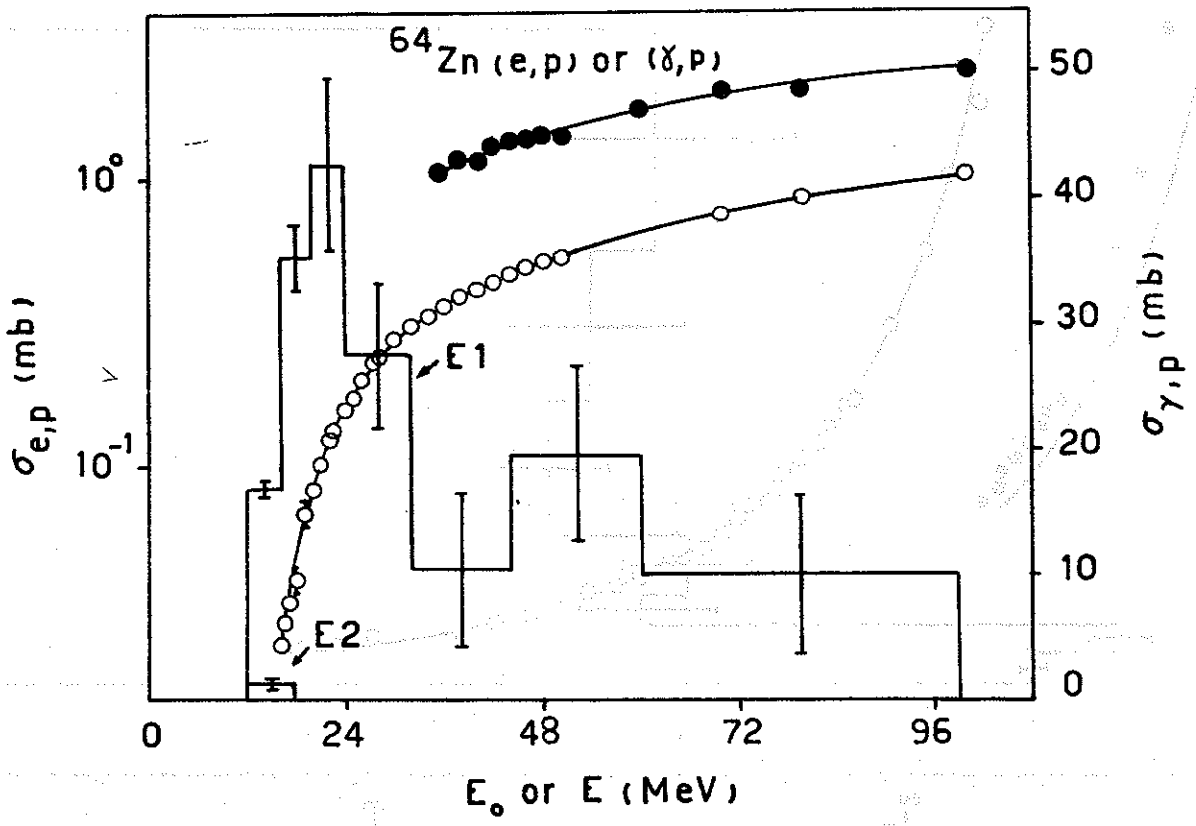
64Zn (e,p) or (γ,p)
E1
E2
10°
10⁻¹
σe,p (mb)
σγ,p (mb)
0
24
48
72
96
E₀ or E (MeV)
50
40
30
20
10
0

Fig.30

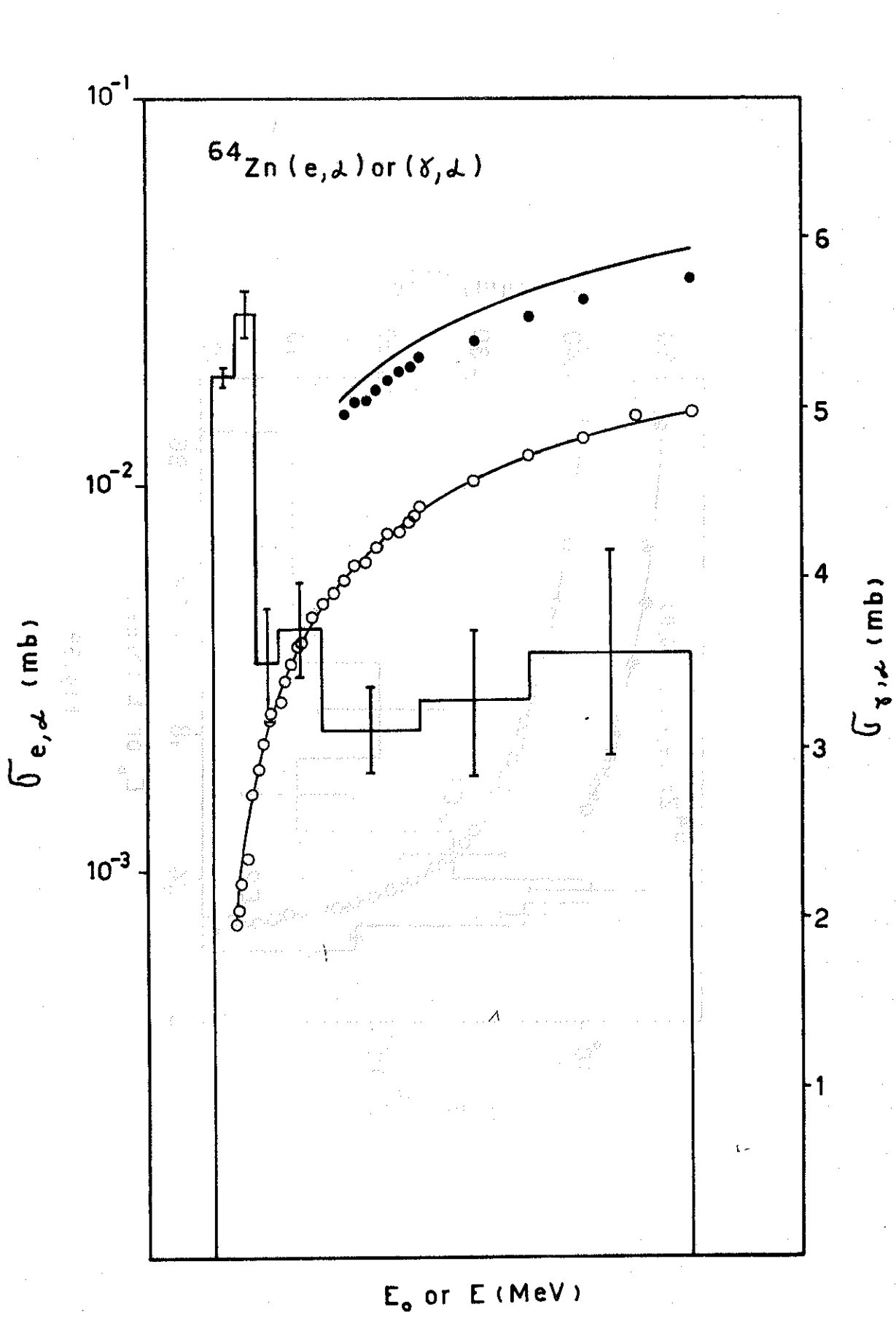
^{64}Zn (e,α) or (γ,α)
10^{-1}
10^{-2}
10^{-3}
$\sigma_{e,\alpha}$ (mb)
$\sigma_{\gamma,\alpha}$ (mb)
6
5
4
3
2
1
E_0 or E (MeV)

Fig.31

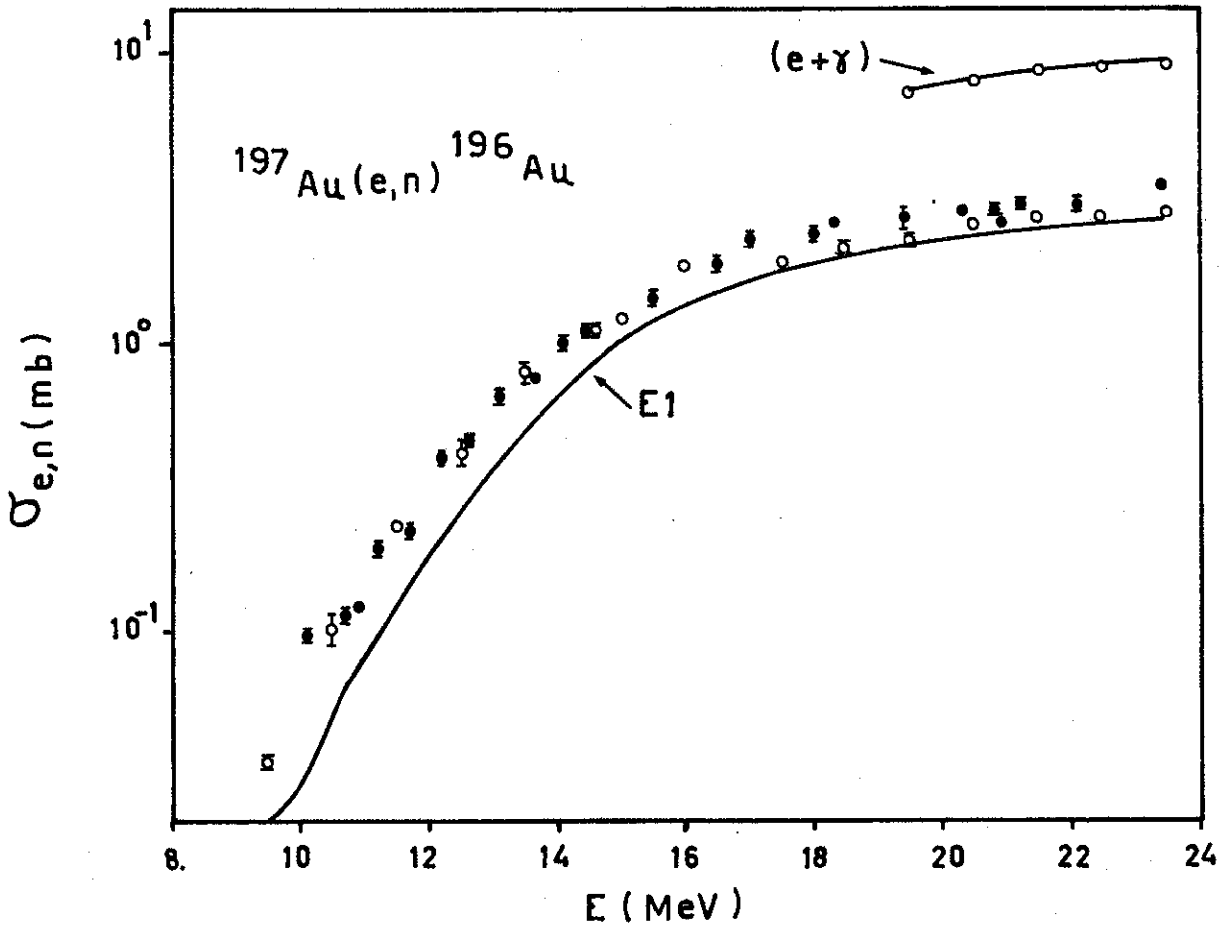
$^{197}Au(e,n)^{196}Au$
(e+γ)
E1
$\sigma_{e,n}$ (mb)
E (MeV)

Fig.32

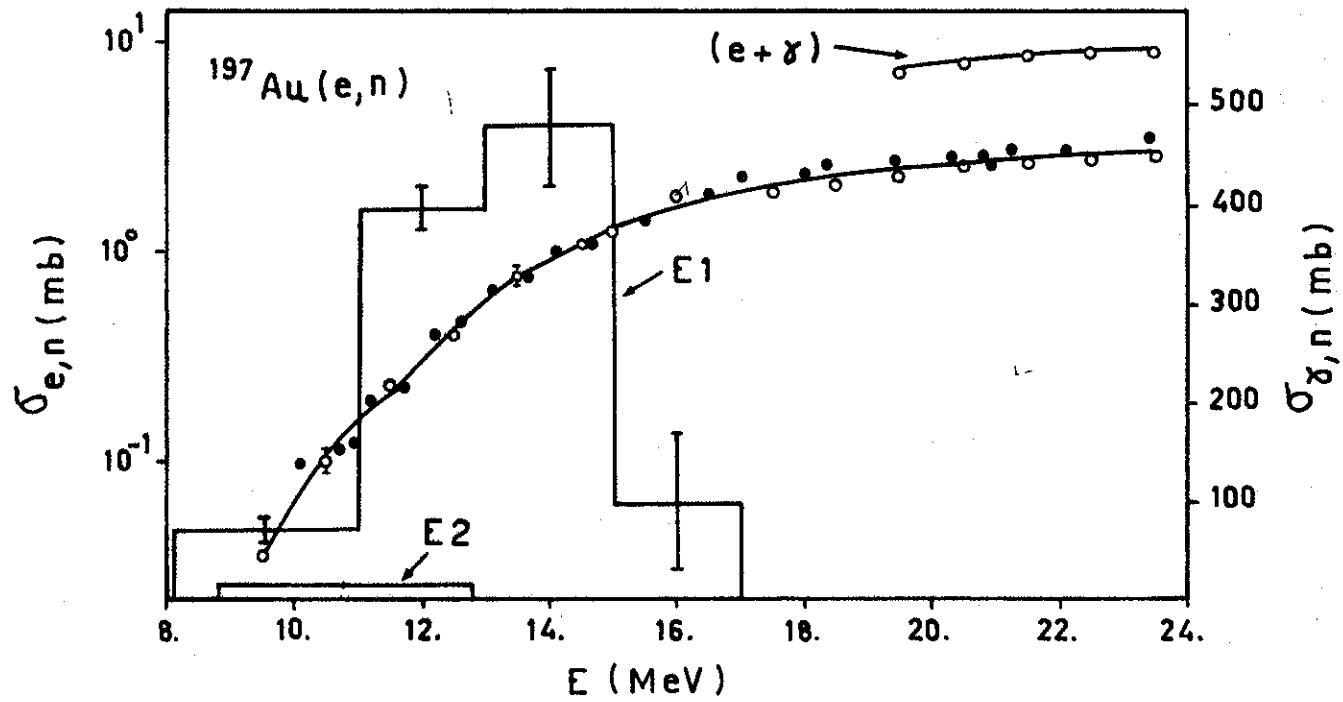
$^{197}Au(e,n)$
(e+γ)
E1
E2
$\sigma_{e,n}$ (mb)
$\sigma_{\gamma,n}$ (mb)
E (MeV)

Fig,33